2011

Numerical Forcing of Horizontally-Homogeneous Stratified Turbulence

Kaustubh J. Rao
University of Massachusetts Amherst, krao@engin.umass.edu

NUMERICAL FORCING OF HORIZONTALLY-HOMOGENEOUS STRATIFIED TURBULENCE

A Thesis Presented

by

KAUSTUBH RAO

Submitted to the Graduate School of the
University of Massachusetts Amherst in partial fulfillment
of the requirements for the degree of

MASTER OF SCIENCE IN MECHANICAL ENGINEERING

May 2011

Mechanical and Industrial Engineering

NUMERICAL FORCING OF HORIZONTALLY-HOMOGENEOUS STRATIFIED TURBULENCE

A Thesis Presented

by

KAUSTUBH RAO

Approved as to style and content by:

_____

Stephen de Bruyn Kops, Chair

_____

David P. Schmidt, Member

_____

Yahya Modarres-Sadeghi, Member

_____

Donald L. Fisher, Department Chair
Mechanical and Industrial Engineering

To my supportive and loving parents, Sandhya Jagannath & H. R. Jagannath

ACKNOWLEDGMENTS

ABSTRACT

NUMERICAL FORCING OF HORIZONTALLY-HOMOGENEOUS STRATIFIED TURBULENCE

MAY 2011

KAUSTUBH RAO

B.E., UNIVERSITY OF MUMBAI

M.S.M.E., UNIVERSITY OF MASSACHUSETTS AMHERST

Directed by: Professor Stephen de Bruyn Kops

It is often desirable to study simulated turbulent flows at steady state even if the flow has no inherent source of turbulence kinetic energy. Doing so requires a numerical forcing scheme and various methods have been studied extensively for turbulence that is isotropic and homogeneous in three dimensions. A review of these existing schemes is used to form a framework for more general forcing methods. In this framework, the problem of developing a forcing scheme in Fourier space is abstracted into the two problems of (1) prescribing the spectrum of the input power and (2) specifying a force that has the desired characteristics and that adds energy to the flow with the correct spectrum. The framework is used to construct three forcing schemes for horizontally homogeneous and isotropic, vertically stratified turbulence. These schemes are implemented in large-eddy simulations and their characteristics analyzed. Which method is "best" depends on the purpose of the simulations, but the framework for specifying forcing schemes enables a systematic approach for identifying a method appropriate for a particular application.

TABLE OF CONTENTS

LIST OF TABLES

LIST OF FIGURES

CHAPTER 1

INTRODUCTION

Turbulence is a non-linear phenomenon occurring in almost every aspect of nature that involves fluids. While an exact definition of turbulence is elusive, turbulent flows are recognized by chaotic-like velocity fluctuations in time and space, existence of a range of scales of motions and kinetic energy dissipation [Pope, 2000]. Turbulence usually stems from some instability in the fluid flow. For example, in homogeneous flows the instability arises from the destabilizing inertial forces overcoming the stabilizing viscous forces. The ratio of inertial to viscous forces known as Reynolds number (Re) gives an estimate on the instability, thereby giving a measure on the turbulent intensity of the flow. In the case of density stratified flows, in addition to viscosity, gravitational forces act as stabilizing forces. Density stratified flows are characterized by density gradients in the vertical direction leading to the formation of distinct density layers. Gravity plays an important role in the formation of layers and gives rise to buoyancy forces. Stratified flows are marked with intermittent patches of turbulence arising due to buoyancy forces. Strength of stratification is measured by the ratio of inertial to gravitational forces, known as Froude number (F_h).

$$\mathrm{F}_h = \frac{\mathcal{U}}{N\mathcal{L}}. \tag{1.1}$$

$\mathcal{L}$ is the horizontal length scale into which energy is assumed to be fed, $\mathcal{U}$ is the corresponding horizontal velocity scale (rms velocity) and $N = (-\,(g/\rho_0)\,(d\tilde{\rho}/dz))^{1/2}$, is the buoyancy frequency also known as the Brunt-Väisälä frequency. The requirement for stratified turbulence is that $\mathrm{F}_h \ll 1$.

A characteristic of the simplest canonical, or building block flows useful in research is that they are inherently dissipative due to viscosity and as a result are not stationary. This implies, in addition to the time scale of turbulent structures there exists a decay time scale. However, some canonical flows such as shear layers or channel flow are inherently stationary, also, in nature mean shear and other phenomena provide continual sources of turbulent kinetic energy to balance energy dissipation. These flows are often approximated to be statistically stationary on time scales that are longer compared to the time scales of turbulence. The question arises as to whether to study turbulent flows that lack a source of energy in their canonical form, that is, decaying in time, or to artificially force them to be statistically stationary. Both approaches have strengths and weaknesses.

Consider, for example, the simplest of all canonical turbulent flows, isotropic homogeneous turbulence [Pope, 2000]. In a laboratory, the flow is well approximated far downstream of a grid in a wind tunnel such as in the experiments of Comte-Bellot and Corrsin [1971]. Producing a direct numerical simulation of that experiment with the correct energy decay rate requires including in the simulation length scales that are much larger than the integral scale of the turbulence [de Bruyn Kops and Riley, 1998], and even then the simulation results have anomalies that appear to stem from the initialization technique and the finite size of the computational domain [Wang and George, 2002]. Therefore, despite the use of the best techniques known and significant computational resources, simulations of the most basic of turbulent flows do not necessarily yield results that are as close to the canonical case as one might like. Forcing the simulated flow to be statistically stationary through the addition of energy at the largest length scales breaks the link between the simulations and a realizable laboratory experiment and introduces an arbitrary forcing mechanism, but it eliminates the time scale of the energy decay which is so hard to get right in simulations of the decaying flow. It also eliminates the need to devote considerable computation effort to computing the flow at length scales much larger than the integral scale.

In turbulence subject to strong stable stratification, one of the simplest canonical flow configurations is horizontally homogeneous and isotropic with a density gradient in the vertical direction. As with unstratified flows, simulating the "correct" temporal development of the flow might be a distraction from understanding other aspects of the flow physics. Riley and de Bruyn Kops [2003] ran simulations of a decaying flow based on turbulence downstream of a grid in a stratified tank. The simulations developed many characteristics observed in laboratory experiments but for a signification portion of the total simulation time the flow was either strongly influenced by the initial conditions or else had lost too much energy to have useful statistics. Lindborg [2006] simulated horizontally-homogeneous stratified turbulence forced to stationarity using a stochastic technique. In that paper, detailed characteristics of the forcing scheme were not highly relevant and were omitted. The study of stratified turbulence using numerical simulations of flows with no intrinsic source of turbulence kinetic energy, however, requires a full understanding of the effects of the forcing, which is the focus of this thesis.

The outline of the thesis is as follows. In section 1.1, a historical review of forcing schemes is presented with emphasis on unstratified turbulence since most work on forcing techniques has been focused on that flow regime. A generic framework for numerical Fourier space forcing is proposed in section 1.2. In chapter 2, basic equations are presented with emphasis on the Boussinesq approximation of Navier-Stokes equation. In chapter 3, the importance of discrete time in numerical simulations is revealed and the theory for random and deterministic Fourier space forcing of horizontally homogeneous stratified turbulence is developed. In chapter 4, appropriate simulation parameters for the forcing schemes developed are enlisted to enable their comparison with reference to Lindborg [2006] simulations. Finally, characteristics of the forcing schemes in terms of the temporal accuracy, the rate of convergence to a statistically stationary state and conclusions are drawn in the chapter 5.

1.1 Background on Forcing Schemes

Historically, the credibility of numerical simulations of fluid flows has depended on favorable comparisons between the simulation results and measurements of physical flows. While acceptance has increased of simulations that are not referenced to specific measurements, it is nevertheless highly desirable to match simulations to laboratory flows. Doing this for statistically stationary flows outside of boundary layers is a challenge, but some progress has been made in developing laboratory experiments in turbulence that is mechanically forced [Hwang and Eaton, 2004; Variano and Cowen, 2008; Variano et al., 2004], and in simulations with stochastic real-space forcing [Lundgren, 2003; Perot, 2010(submitted); Rosales and Meneveau, 2005]. The most common approach to applying forcing in simulations of unbounded turbulent flows, however, is to do so in Fourier space. The drawback is that the simulations are not realizable in the laboratory but the methodology is well-supported by theory.

A review of Fourier-space forcing schemes reveals desirable characteristics of forcing techniques along with several pitfalls. Kuczaj and Geurts [2006] note that forcing techniques can be designed to add constant power or to maintain constant energy in, say, a range of wave numbers. Forcing can then be implemented via a stochastic approach or a deterministic one. One of the earliest forcing schemes sought to maintain the kinetic energy in the flow stationary by freezing the amplitude of the velocity in all modes with wave number magnitude in a given range, that is, in a particular "wave number band" [Siggia and Patterson, 1978]. This approach requires knowing *a priori* the desired energy in those modes and precludes any affect of motions at small length scales on the dynamics of the large length scales. Chasnov [1991] relaxes the latter constraint by requiring that the average energy in a wave number band be held fixed while allowing the energy in each mode to vary. Unfortunately, schemes of this type suffer from large excursions of the average kinetic energy of the flow in the process of converging [Sullivan et al., 1994; Vincent and Meneguzzi, 1991]. Alternative approaches hold constant the average energy in the flow [Gross-

4

mann and Lohse, 1992; Machiels, 1997] and allow the spectrum to evolve to stationarity, which can result in large excursions of the energy at particular wave numbers.

To address the problems with slow convergence and large energy fluctuations that are common to many schemes, Overholt and Pope [1998] force the flow toward the prescribed energy spectrum over some range of wave numbers but do not require that the target energy spectrum be matched exactly. Instead, a spring-damper analogy is used to construct differential equations for each band of wave numbers, the equations are tuned to be approximately critically damped, and their solutions are used to determine the force magnitudes at each time step. The forcing results in the energy spectrum of the flow optimally approaching the target.

In addition to having a mechanism for determining how much power to add to the flow and at what wave number bands, a forcing scheme must include a process for distributing the energy across the individual modes that make up a band. In the earliest schemes the modes were simply frozen. Many later schemes used linear amplification of the existing velocity field [Kerr, 1981; Overholt and Pope, 1998; Vincent and Meneguzzi, 1991]. This approach of adding energy by scaling existing velocities allows the large scales of the flow to evolve in time but it is not clear that the resulting simulation will be statistically stationary, and also large scale anisotropies are frozen [Vincent and Meneguzzi, 1991]. The method of Overholt and Pope uses linear amplification but the amplification factor is dynamically controlled to improve convergence.

Stochastic approaches can also be used to distribute the forcing power across multiple wave number modes. This avoids some of the problems associated with linear amplification. One of the first stochastic forcing schemes for homogeneous isotropic turbulence is that of Eswaran and Pope [1988]. In this approach, random acceleration forces are added when the velocities for the wave number modes being forced are advanced in time. Constraints are imposed so that the resulting velocity field remains non-divergent and that the forces are applied at the desired length scales for the desired duration.

In most of the schemes just considered, the kinetic energy is prescribed in one way or another. This is appropriate for flows for which theory is sufficiently developed to guide the selection of the target energy. The theory of stratified turbulence has not advanced to the point of providing such guidance. In fact, only recently has it been shown that energy input at the large scales of a stratified flow cascades to the small scales [Lindborg, 2006; Riley and de Bruyn Kops, 2003]. Therefore, a class of forcing schemes where power input is prescribed is attractive for simulations of stratified turbulence.

Ghosal et al. [1995] developed a non-stochastic, constant-power scheme in which linear amplification is used to add energy to the flow. Stationarity is observed when dissipation rate fluctuates about the constant power input. Very high energy levels and associated numerical problems can result with schemes of this type because of the time required for the turbulence cascade to develop. As with the constant-energy approaches, the side-effects of linear amplification can be ameliorated by stochastic methods [Carati et al., 1995; Misra and Pullin, 1997]. Methods have also been developed in which both the input power and the distribution of the input power across several wave number bands are prescribed [Chen, 1992; Wang et al., 1996].

Most of the work on forcing schemes have been focused on isotropic homogeneous flows. Numerical forcing of stratified flows is fairly recent and requires research. For the same, Lindborg [2006] approximates stratified flows to be horizontally-homogeneous and isotropic while using a variant of Alvelius forcing scheme to force just horizontal modes of horizontal velocity components. In this thesis a generic framework for Fourier space numerical forcing is developed and Lindborg [2006] simulations are reproduced. Thus proving that the framework is not limited only to the regime of isotropic homogeneous flows.

1.2 General Framework for Fourier Space Numerical Forcing

The preceding review reveals that the development of a Fourier-space forcing scheme is composed of two subproblems: determining how much energy to add to each wave number band and how to distribute the energy among the modes that make up each band. In this section, a framework is developed that enables the two subproblems to be addressed systematically. Before the framework is introduced it is important to consider the discrete time aspect of numerical forcing.

A characteristic of many forcing schemes is that they are derived in terms of equations that are continuous in time. Forcing is done by appending an artificial force term to the Navier-Stokes time-continuous momentum equation. The nature of the force is described by it's orientation and phase with respect to velocity. The addition of a force term in the momentum equation results in a spatial force-velocity correlation term in the kinetic energy equation. This implies, only a force that correlates with velocity can contribute to input power. In other words, only a force parallel-in-phase with velocity can contribute to kinetic energy. Alvelius [1999] considers the discrete nature of time in numerical simulations and reveals the existence of an additional spatial force-force correlation term that contributes to kinetic energy. This term has no analog in the time-continuous evolution of kinetic energy and arises as a result of the force being constantly applied over the discrete interval of time. Due to the existence of this term, forces that do not correlate spatially with velocity can also inject power, hence forces that are perpendicular and parallel-out-of-phase with velocity can also contribute to kinetic energy. Thus the input power is considered to have contributions from forces perpendicular, parallel-out-of-phase and parallel-in-phase with velocity.

In section 3.2.1 it is shown for a prescribed distribution of power, the individual contributions to power by forces that correlate with velocity and those that don't can be controlled. The forcing scheme by Alvelius can be considered to avail a special case of this control, where contribution to power by force-velocity correlation is set to zero, thereby injecting power solely through force-force correlation. With this control, the problem of prescribing power is now isolated from prescribing the nature of force. This allows the framework for numerical forcing to be formulated
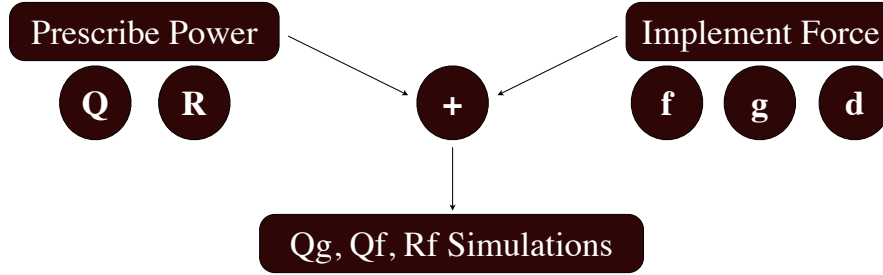
Figure 1.1. Figure shows the new framework for numerical forcing schemes.

as three addition steps. First, power is prescribed. For example, the power prescribed can have a constant wave-number distribution or adapt with time by a control equation [section 3.2.2]. Second, the nature (orientation and phase) of force is chosen [section 3.2.1]. Lastly, combine the first two steps into a practical algorithm constituting a simulation [section 3.2.3]. This framework is summarized in figure 1.1, where "Q" or "R" represent two ways to prescribe power and "f","g" and "d" represent three kinds of forces detailed in chapter 3.

1.3 Numerical Forcing of Horizontally-Homogeneous Stratified Flows

The framework developed in this thesis is proved by successfully forcing horizontally-homogeneous stratified flow into a statistical steady state. To force such flows requires the force to be isotropic and homogenous in the horizontal plane while ensuring the velocity field remain non-divergent. In Fourier space this is achieved by forcing only the horizontal components of velocity in the horizontal plane $\kappa_3 = 0$. This makes the system highly constrained and as a result, force perpendicular to velocity cannot exist and the directional degree of freedom for choosing force is lost. This leaves only the phase and magnitude of the force to be modeled or stochastically assigned.

Numerical simulations run by Lindborg [2006] pertain to forcing horizontally-homogeneous stratified flows. These simulations are reproduced by developing a Qg scheme that is a specific case of the generic framework. The scheme takes advantage of the fact that for discrete time it

is possible to inject power by spatial force-force correlation. The Qg scheme uses a "g" force that does not correlate with velocity. Since the power injected by the g force is an artifact of discretization, it is not desirable to have this force correlate in time with itself. To ensure this, stochastic processes similar to Alvelius is used.

The physical implications for an out-of-phase force (g force) is unclear. In order to justify that numerical forcing is a surrogate for slowly-developing large scales, two new forcing schemes are developed that utilize an "f" force that is spatially correlated with velocity. These are presented as specific cases of the framework. The first scheme termed as the Qf scheme, injects a constant power distribution similar to Qg scheme. The mechanism of input power distribution for both the Qg and Qf is constant and independent of the runtime flow dynamics. As a result, slow convergence to steady state is observed. To address this, a second "Rf scheme" based on Overholt and Pope [1998] is developed. In this scheme the mechanism of input power uses a control system that takes into account information from runtime flow dynamics (spectrum of kinetic energy at $\kappa_3 = 0$ plane). Based on this information the distribution of input power among horizontal wave-number bands is accordingly adjusted to converge the flow to a given target spectrum. As expected, convergence to steady state is observed to be faster. This method, however requires a target spectrum to be provided, which for the horizontally-homogeneous stratified flow, does not exist. However, to test the methodology a target spectrum is acquired from the converged solutions of the Qf scheme.

CHAPTER 2

THEORETICAL CONSIDERATIONS

This chapter defines terminology and nomenclature for various physical quantities that enable mathematical representation of forcing schemes. A brief overview on equations in physical space and Fourier space is given. A fluid flow can be expressed by conservation equations. These equations represent the balances, changes and fluxes of physical quantities pertaining to fluid flow with respect to space and time. The fundamental governing equations of a fluid element are the continuity, momentum and internal energy equation along with the equation of state. Using these equations, equations for potential and kinetic energy can be derived. For detailed derivations, refer Kundu and Cohen [2002]; Panton [1984]; Pope [2000]; Spiegel and Veronis [1960].

2.1 General Continuity Equation

Consider a material region $(\mathcal{M})$. Let dV be an infinitesimal volume with density ρ_t. As mass is conserved for all time, the rate of change of mass (M) of the material region (system) is zero. This is mathematically expressed as,

$$\frac{D}{Dt}\left(M_{\mathcal{M}}\right) = \frac{D}{Dt}\left(\int_{\mathcal{M}} \rho_t dV\right) = 0 \,, \tag{2.1}$$

where $D(\cdots)/Dt$ is the material derivative. Using Leibnitz's theorem to take the differential operator inside the integral and using Gauss theorem gives,

$$\frac{\partial \rho_t}{\partial t} + \frac{\partial}{\partial x_i}\left(\rho_t u_i\right) = 0 \,. \tag{2.2}$$

u_i is i^{th} component of the velocity vector ($\vec{u}$) of the fluid element. This is the mass conservation equation or continuity equation for a fluid system in the domain of continuum mechanics [Panton, 1984].

2.2 General Momentum Equation

The momentum equation can be derived based on Newton's second law. For detailed derivation, refer appendix A and Panton [1984]. If external force $\vec{b}$ and gravity $\vec{g} = [0, 0, g]$ are the only body forces per unit mass then the general momentum equation is,

$$\frac{\partial}{\partial t}\left(\rho_t u_i\right) + \frac{\partial}{\partial x_j}\left(\rho_t u_j u_i\right) = -\frac{\partial p_t}{\partial x_i} + \rho_t\left(-g\delta_{i3} + b_i\right) + \frac{\partial \tau_{ij}}{\partial x_j}\ ,\qquad (2.3)$$

where τ_{ij} is a symmetric viscous tensor. The Navier-Stokes momentum equation obtained by substituting equation (A.10) for τ_{ij} is,

$$\frac{\partial}{\partial t}\left(\rho_t u_i\right) + \frac{\partial}{\partial x_j}\left(\rho_t u_j u_i\right) = -\frac{\partial p_t}{\partial x_i} + \rho_t\left(-g\delta_{i3} + b_i\right) + 2\frac{\partial}{\partial x_j}\left(\mu S_{ij}\right) - \frac{2}{3}\frac{\partial}{\partial x_i}\left(\mu\frac{\partial u_j}{\partial x_j}\right)\ .\quad (2.4)$$

p_t is the thermodynamic pressure, μ is molecular viscosity, g is the magnitude of gravitational acceleration and S_{ij} is the symmetric strain rate tensor (defined in equation (A.8)). Forcing schemes (discussed in chapter 3) acheive statistical steady by modeling the external force term $\vec{b}$ appended to the momentum equation.

2.3 General Internal Energy Equation

Internal energy of the fluid particle is due to microscopic motions. These include translational, vibrational and rotational motions. The sum of all these energies is the absolute thermodynamic internal energy. The internal energy per unit mass is,

$$de \equiv C_v dT\ ,\qquad (2.5)$$

where C_v is the specific heat at constant volume and dT is an infinitesimal change in temperature.

Internal energy of a system can change as a result of energy flux across the surface boundary of the system. Energy flux occurs due to heat transfer by conduction, convection, radiation or diffusion of different chemical species. Heat transfer is given by, $-n_i q_i d\mathcal{S}$, where $\vec{q}$ denotes the heat flux per unit mass across surface element $d\mathcal{S}$ having outward normal $\vec{n}$. Heat flux is defined as

$$q_i \equiv -k_T \frac{\partial T}{\partial x_i} \, , \qquad (2.6)$$

where k_T is the thermal conductivity of the fluid element. The equation for internal energy is,

$$\frac{\partial}{\partial t} (\rho_t e) + \frac{\partial}{\partial x_i} (\rho_t u_j e) = \frac{\partial}{\partial x_i} \left(k_T \frac{\partial T}{\partial x_i} \right) - p_t \frac{\partial u_i}{\partial x_i} + \tau_{ij} \frac{\partial u_i}{\partial x_j} \, . \qquad (2.7)$$

Internal energy cannot be measured directly, instead it is inferred from measuring temperature. Thus it is convenient to cast the above equation in terms of temperature. Referring to appendix B for derivation and noting

$$\rho_t : \rho_t (p_t, T, \xi) \, , \qquad (2.8)$$

the internal energy equation in terms of temperature is,

$$\rho_t C_p \frac{DT}{Dt} = \frac{\partial}{\partial x_i} \left(k_T \frac{\partial T}{\partial x_i} \right) + T \beta_t \frac{Dp_t}{Dt} \, . \qquad (2.9)$$

β_t is the coefficient of thermal expansion, C_p is the specific heat at constant pressure and ξ is entropy per unit mass.

2.4   General Kinetic Energy Equation

The equation for kinetic energy is obtained by the dot product of velocity with the momentum equation (2.3). Using the relation $u_i \partial u_i = (1/2)\partial (u_i u_i)$, the kinetic energy equation is,

$$\frac{\partial}{\partial t}\left(\rho_t \frac{1}{2}u^2\right) + \frac{\partial}{\partial x_i}\left(\rho_t u_j \frac{1}{2}u^2\right) = -u_i \frac{\partial p_t}{\partial x_i} + u_i \frac{\partial \tau_{ij}}{\partial x_j} + \rho_t u_i \left(-g\delta_{i3} + b_i\right) \qquad (2.10)$$

where τ_{ij} is given by equation (A.11), $u = |\vec{u}|$ and $\frac{1}{2}u^2 = \frac{1}{2}u_i u_i$.

2.5   The Boussinesq Approximation

First suggested by Boussinesq [1903], density stratified flows are modeled by the Boussinesq approximation of Navier-Stokes equation (equations (2.13), (2.14) and (2.15)). In the Boussinesq approximation it is assumed that density fluctuations are a result of thermal effects and the accelerations of the fluid element are small compared to that of gravity.

Any physical variable, ψ_t, can be decomposed into three components: spatial average, ψ_o, variation in absence of motion, $\tilde{\psi}$, and fluctuations due to fluid motion, ψ [Spiegel and Veronis, 1960]. Thus density ρ_t and pressure p_t can be decomposed respectively as,

$$
\begin{aligned}
\rho_t\left(\vec{x}, t\right) &= \rho_0 + \tilde{\rho}\left(z\right) + \rho\left(\vec{x}, t\right) \ , \\
p_t\left(\vec{x}, t\right) &= p_o + \tilde{p}\left(z\right) + p\left(\vec{x}, t\right) \ ,
\end{aligned}
\qquad (2.11a)
$$

where z corresponds to depth. In the Boussinesq approximation, terms of order ε are kept, where

$$\varepsilon \equiv \frac{\Delta\tilde{\rho}}{\rho_0} \ll 1 \qquad (2.12)$$

and $\Delta\tilde{\rho} = \left(\tilde{\rho}_{max} - \tilde{\rho}_{min}\right)$ is the maximum variation in density.

The Boussinesq approximation of the continuity, density, momentum and kinetic energy equation are derived in appendix C. The internal energy equation combined with equation of state gives [refer section C.3.3],

$$\frac{\partial \rho}{\partial t} + u_i \frac{\partial \rho}{\partial x_i} + u_i \frac{d\tilde{\rho}\left(z\right)}{dx_i}\delta_{i3} = D_m \frac{\partial^2 \rho}{\partial x_i^2} \ . \qquad (2.13)$$

$D_m = k_T / (\rho_0 C_p)$ is the mass diffusivity. The continuity equation is (refer section C.3.1),

$$\frac{\partial u_i}{\partial x_i} = 0 \ . \tag{2.14}$$

The momentum equation is (refer section C.3.2),

$$\frac{D u_i}{Dt} = -\frac{1}{\rho_0} \frac{\partial p}{\partial x_i} - \frac{\rho}{\rho_0} g \delta_{i3} + b_i + \nu \frac{\partial^2 u_i}{\partial x_j^2} \ . \tag{2.15}$$

$\nu = \mu / \rho_0$ is the kinematic viscosity (assumed to be a constant). Defining vorticity to be $\omega_i \equiv \varepsilon_{ijk} (\partial u_k / \partial x_j)$ and using the identity,

$$u_j \frac{\partial u_i}{\partial x_j} = -\varepsilon_{ijk} \omega_j u_k + \frac{1}{2} \frac{\partial}{\partial x_i} (u_j u_j) \ , \tag{2.16}$$

the momentum equation (2.15) in terms of vorticity is,

$$\left(\frac{\partial}{\partial t} - \nu \frac{\partial^2}{\partial x_j^2} \right) u_i = \varepsilon_{ijk} u_j \omega_k - \frac{\partial}{\partial x_i} \left(\frac{1}{\rho_0} p + \frac{1}{2} u_j u_j \right) + b_i - \frac{\rho}{\rho_0} g \delta_{i3} \ . \tag{2.17}$$

The momentum equation is conveniently written as,

$$\frac{\partial u_i}{\partial t} = A_i + Z_i + D_i + b_i - B_i \ . \tag{2.18}$$

Where,

$$\begin{aligned}
A_i &\equiv \varepsilon_{ijk} u_j \omega_k \ . \\
Z_i &\equiv -\frac{\partial}{\partial x_i} \left(\frac{1}{\rho_0} p + \frac{1}{2} u^2 \right) \ , \\
D_i &\equiv \nu \frac{\partial^2}{\partial x_j^2} u_i \ , \\
B_i &\equiv \frac{g_i}{\rho_0} \rho \delta_{i3} \ .
\end{aligned} \tag{2.19}$$

A_i represents advection of momentum, Z_i is the gradient of the modified pressure, D_i represents the viscous diffusion of momentum and B_i is the gravity term.

14

The kinetic energy equation from equations (C.22) and (C.23) is

$$\frac{\partial \mathcal{E}_k}{\partial t} + u_j \frac{\partial \mathcal{E}_k}{\partial x_j} = -\frac{u_i}{\rho_0}\frac{\partial p}{\partial x_i} - \frac{\rho}{\rho_0}u_i g\delta_{i3} + u_i b_i + 2\nu\frac{\partial}{\partial x_j}\left(u_i S_{ij}\right) - \epsilon_k \,, \tag{2.20}$$

where $\mathcal{E}_k = \frac{1}{2}u^2$ is the kinetic energy per unit mass, ϵ_k, defined in equation (C.24), is the dissipation of kinetic energy (refer section C.3.4). The term, $(\rho/\rho_0)u_i g\delta_{i3} = (\rho/\rho_0)gu_3$ is known as the buoyancy flux term. It acts as a coupling term between kinetic and potential energy by transferring energy back and forth between these two forms of energy.

By using the Boussinesq approximation, it is assumed that density fluctuations are only due to temperature fluctuations and not due to pressure effects. With this assumption the internal energy equation (2.9) simplifies to

$$\rho_t C_p \frac{DT}{Dt} = \frac{\partial}{\partial x_i}\left(k_T \frac{\partial T}{\partial x_i}\right) \,. \tag{2.21}$$

2.6 Potential Energy

In this section the evolution of potential energy equation is given and the corresponding terms are defined. For more details refer Holliday and McIntyre [1981]; Lorenz [1955]; Winters et al. [1995].

The evolution equation for potential energy can be obtained by multiplying equation (2.13) with ρ and appropriately scaling so that the buoyancy flux term appearing in the kinetic energy equation (2.20) and potential energy equation (2.22) are identical and of opposite signs. The equation for potential energy obtained is,

$$\frac{\partial \mathcal{E}_p}{\partial t} + u_i \frac{\partial \mathcal{E}_p}{\partial x_i} = \frac{g}{\rho_0}\rho u_i \delta_{i3} + D_m \frac{\partial^2 \mathcal{E}_p}{\partial x_i^2} - \epsilon_p \tag{2.22}$$

where,

$$\mathcal{E}_p = \frac{-g}{2\rho_0 \frac{d\tilde{\rho}}{dz}}\rho^2 \tag{2.23}$$

is the available potential energy of the fluid element and

$$\epsilon_p = -\frac{g}{\rho_0 \frac{\partial \tilde{\rho}}{dz}} D_m \frac{\partial \rho}{\partial x_i} \frac{\partial \rho}{\partial x_i} \ , \tag{2.24}$$

is the dissipation of potential energy.

2.7 Contributions to Kinetic Energy

Total kinetic energy can be decomposed into contributions by horizontal and vertical velocity components. The contribution to kinetic energy by horizontal velocity components gives the horizontal contribution to kinetic energy, $\mathcal{E}_h$. Similarly, contribution by the vertical component of velocity gives vertical contribution to kinetic energy, $\mathcal{E}_v$. For research purposes, the simplest density stratified flows considered are horizontally-homogeneous and isotropic. Decomposing kinetic energy into $\mathcal{E}_h$ and $\mathcal{E}_v$ gives a better understanding of the energetics the flow and terms responsible for the transfer of energy between $\mathcal{E}_h$ and $\mathcal{E}_v$ become apparent. Mathematical expressions for $\mathcal{E}_h$ and $\mathcal{E}_v$ are derived in appendix D.

$$\begin{aligned}
\mathcal{E}_h &\equiv \tfrac{1}{2}\left(u_1 u_1 + u_2 u_2\right) \ , \\
\mathcal{E}_v &\equiv \tfrac{1}{2} u_3 u_3 \ , \\
\mathcal{E}_k &= \mathcal{E}_h + \mathcal{E}_v \ .
\end{aligned} \tag{2.25a}$$

Horizontal components are denoted by subscript $_h$. For a vector $(\vec{\cdot})_h$ implies index $h = 1, 2$. With this notation, horizontal component of velocity is, $u_h = [u_1, u_2]$ and $\mathcal{E}_h = (1/2)u_h u_h$. Vertical components are denoted by subscript $_v$ and for a vector $(\vec{\cdot})_v = (\vec{\cdot})_3$ and $\mathcal{E}_v = (1/2)u_3 u_3$.

The horizontal and vertical contributions to kinetic energy are derived in appendix D. The equation for the horizontal contribution to kinetic energy $(\mathcal{E}_h)$ is,

$$\frac{\partial \mathcal{E}_h}{\partial t} + u_h \frac{\partial \mathcal{E}_h}{\partial x_h} + u_3 \frac{\partial \mathcal{E}_h}{\partial x_3} = -\frac{u_h}{\rho_0} \frac{\partial p}{\partial x_h} + b_h u_h + 2\nu \frac{\partial}{\partial x_j} \left(u_h S_{hj} \right) \tag{2.26}$$

$$- 2\nu S_{hj} S_{hj} + 2\nu \left(S_{13} r_{13} + S_{23} r_{23} \right) ,$$

where r_{ij} is the angular deformation rate tensor. The vertical contribution to kinetic energy $(\mathcal{E}_v)$ is

$$\frac{\partial \mathcal{E}_v}{\partial t} + u_h \frac{\partial \mathcal{E}_v}{\partial x_h} + u_3 \frac{\partial \mathcal{E}_v}{\partial x_3} = -\frac{u_3}{\rho_0} \frac{\partial p}{\partial x_3} - \frac{\rho}{\rho_0} u_3 g + b_v u_3 + 2\nu \frac{\partial}{\partial x_j} \left(u_3 S_{3j} \right) \tag{2.27}$$

$$- 2\nu S_{3j} S_{3j} - 2\nu \left(S_{13} r_{13} + S_{23} r_{23} \right) .$$

By decomposing $\mathcal{E}_k$ into $\mathcal{E}_h$ and $\mathcal{E}_v$ contributions (equations (2.26) and (2.27)), the existence of $2\nu \left(S_{13} r_{13} + S_{23} r_{23} \right)$ term is revealed. Observing the sign of this term in both the equations, it appears to be a viscous coupling term between horizontal and vertical contribution to kinetic energy.

2.8 Spectral Equations

Fourier space numerical forcing requires Fourier transforming the basic equations in the three spatial directions. In this section the mathematical terminology used to describe and quantify Fourier space quantities is presented.

Let $(\hat{\cdot})$ denote Fourier transform along the three spatial directions of $(\cdot)$. The Fourier transform of the continuity equation (2.14) is,

$$\kappa_i \hat{u}_i = 0 . \tag{2.28}$$

κ_i is the ith component of the three dimensional wave-vector, $\vec{\kappa}$. The Fourier transform of the momentum equation (2.18) is,

$$\frac{\partial}{\partial t} \hat{u}_i(\vec{\kappa}, t) = \hat{A}_i(\vec{\kappa}, t) - \hat{B}_i(\vec{\kappa}, t) + \hat{Z}_i(\vec{\kappa}, t) + \hat{b}_i(\vec{\kappa}, t) + \hat{D}_i(\vec{\kappa}, t) . \tag{2.29}$$

17

Eliminating the $\hat{Z}_i$ term, the Fourier space momentum equation for forced density stratified flows is (refer appendix E),

$$\frac{\partial \hat{u}_i}{\partial t} = \Lambda_{ij} \left(\hat{A}_j - \hat{B}_j \right) - \nu\kappa^2 \hat{u}_i + \hat{b}_i \, . \tag{2.30}$$

$\hat{\vec{A}} \equiv \widehat{(\vec{u} \times \vec{\omega})}$, $\Lambda_{ij} \equiv [\delta_{ij} - (\kappa_i \kappa_j)/\kappa^2]$ and $\kappa \equiv |\vec{\kappa}|$ is the magnitude of the wave-vector. The momentum equation (2.30) is conveniently written as,

$$\frac{\partial \hat{u}_i(\vec{\kappa}, t)}{\partial t} = \hat{a}_i(\vec{\kappa}, t) + \hat{b}_i(\vec{\kappa}, t) \tag{2.31}$$

where $\hat{b}_i$ is the forcing term and $\hat{a}_i$ represents the contribution from Navier-Stokes accelerations.

Let $(\cdot)^*$ denote complex-conjugate. The equation for Fourier space kinetic energy ($\hat{E}_k \equiv \hat{u}_i \hat{u}_i^*/2$) is obtained by the dot product of equation (2.30) with the complex-conjugate of velocity vector ($\hat{u}_i^*$). Equation for $\hat{E}_k$ derived in section E.2 restated is,

$$\frac{\partial \hat{E}_k(\vec{\kappa}, t)}{\partial t} = \Lambda_{ij} \left(\hat{A}_j - \hat{B}_j \right) \hat{u}_i^* + \hat{b}_i \hat{u}_i^* - \nu\kappa^2 \hat{E}_k \, . \tag{2.32}$$

The equation for Fourier space kinetic energy is conveniently written as,

$$\frac{\partial \hat{E}_k(\vec{\kappa}, t)}{\partial t} = \hat{T}_k(\vec{\kappa}, t) - \hat{T}_B(\vec{\kappa}, t) + \hat{T}_b(\vec{\kappa}, t) + \hat{T}_{\epsilon_k}(\vec{\kappa}, t) \, . \tag{2.33}$$

Where $\hat{T}_k(\vec{\kappa}, t)$ is a non-linear term responsible for transferring energy from low wave numbers to high wave numbers or, in other words, transferring energy from large scales to smaller scales of motion. $\hat{T}_b(\vec{\kappa}, t)$ is the injected power due to forcing, $\hat{T}_B(\vec{\kappa}, t)$ is the buoyancy flux term and $\hat{T}_{\epsilon_k}(\vec{\kappa}, t)$ is the Navier-Stokes dissipation term. These terms are defined in appendix E, equation (E.14).

The Fourier transform of density equation (2.13) multiplied with scaling constant $\mathcal{C} = -g/\left(2\rho_0(d\tilde{\rho}/dz)\right)$ is,

$$\mathcal{C}\frac{\partial \hat{\rho}}{\partial t} + \left(\widehat{\mathcal{C}u_i\frac{\partial \rho}{\partial x_i}}\right) - \frac{g}{\rho_0}\hat{u}_3 = -\mathcal{C}D_m\kappa^2\hat{\rho}\,. \tag{2.34}$$

The above equation is multiplied by the complex conjugate of $\hat{\rho}$ (refer appendix E, section E.3) to give the Fourier space equation of available potential energy $(\hat{E}_p)$,

$$\frac{\partial \hat{E}_p(\vec{\kappa},t)}{\partial t} = -\hat{T}_p(\vec{\kappa},t) + \hat{T}_B(\vec{\kappa},t) + \hat{T}_{\epsilon_p}\,. \tag{2.35}$$

$\hat{T}_p$ is the transfer of potential energy, $\hat{T}_B$, discussed earlier is the buoyancy flux term and $\hat{T}_{\epsilon_p}$ is the dissipation of potential energy. These terms are defined in appendix E, equation (E.19).

CHAPTER 3

FORCING METHODOLOGY

This chapter presents a general framework for numerical forcing in Fourier space. Numerical forcing in Fourier space can be decomposed into two isolated problems, namely determining the distribution of energy over wave-number bands and how to distribute energy among the modes that make up each band. Three forcing schemes are developed as specific cases of this framework. However, before introducing the framework, the importance of considering discrete time in numerical simulations is first discussed.

3.1   Importance of Discrete Time

A characteristic of many forcing schemes is that they are derived in terms of equations that are continuous in time. In continuous time domain, power can only be injected via a spatial force-velocity correlation. From equation (2.20), this can be achieved only by a force parallel-in-phase with velocity. Alvelius [1999] considers the discrete nature of time in the time evolution of energy and reveals the existence of an additional spatial force-force correlation term that also contributes to adding energy. This term has no analog in the time-continuous evolution of energy and arises as a result of the force being constantly applied over a discrete interval of time. The existence of an additional force-force correlation term allows three possible sources of input power. These are, force perpendicular, in-phase-parallel and out-of-phase-parallel to velocity.

3.1.1 Spatial Correlation of Force

An important aspect that results from discretizing time is the contribution to power by spatial force-force correlation. Let $\vec{a}$ represent all the Navier-Stokes acceleration terms in momentum equation (2.18) giving,

$$\frac{\partial u_i(\vec{x}, t)}{\partial t} = a_i(\vec{x}, t) + b_i(\vec{x}, t) . \tag{3.1}$$

To simplify analysis, consider discretizing above equation by an Euler step. Dropping the representation of spatial and temporal dependence yields,

$$u_i^{(n+1)} = u_i^{(n)} + (a_i^{(n)} + b_i^{(n)})\Delta t . \tag{3.2}$$

Δt is the discrete time-step over which physical terms remain constant and the superscript $^{(n)}$ indicates the discrete time step number $(t^{(n)})$. Average kinetic energy $\langle \mathcal{E}_k \rangle_\ell$ for the $(n+1)^{th}$ time-step is

$$\left\langle \mathcal{E}_k^{(n+1)} \right\rangle_\ell = \frac{1}{2} \left\langle u_i^{(n+1)} u_i^{(n+1)} \right\rangle_\ell .$$

$\langle \cdots \rangle_\ell$ indicates spatial average. Substituting equation (3.2) in the above equation yeilds,

$$\left\langle \mathcal{E}_k^{(n+1)} \right\rangle_\ell = \frac{1}{2} \left[\left\langle u_i^{(n)} u_i^{(n)} \right\rangle_\ell + \left\langle (a_i^{(n)} + b_i^{(n)})^2 \Delta t \Delta t \right\rangle_\ell + 2 \left\langle (u_i^{(n)} a_i^{(n)} + u_i^{(n)} b_i^{(n)})\Delta t \right\rangle_\ell \right] . \tag{3.3}$$

Dropping the $\langle \cdots \rangle_\ell$ notation, the rate of change of kinetic energy is:

$$\frac{\mathcal{E}_k^{(n+1)} - \mathcal{E}_k^{(n)}}{\Delta t} = \frac{\Delta \mathcal{E}_k}{\Delta t} = \left\{ \frac{1}{2} b_i^{(n)} b_i^{(n)} \Delta t + u_i^{(n)} b_i^{(n)} + u_i^{(n)} a_i^{(n)} \right\} + \left[a_i^{(n)} + b_i^{(n)} \right] a_i^{(n)} \Delta t . \tag{3.4}$$

In the above equation, $u_i^{(n)} b_i^{(n)}$ is analogous to $u_i b_i$ term in continuous time kinetic energy equation (2.20). This is the contribution to power by spatial force-velocity correlation. $u_i^{(n)} a_i^{(n)}$ corresponds to the Navier-Stokes energy terms and terms in $[\cdots]$ brackets correspond to first order error terms resulting from Euler discretization. Also present in the above equation is $b_i^{(n)} b_i^{(n)}$ term that has no

analogue in the time continuous equation (2.20). This is the contribution to power by the spatial force-force correlation.

The $b_i^{(n)} b_i^{(n)}$ term is an artifact of discretizing time and is a result of force remaining constant over the discrete interval of time, Δt. To emphasize, assume the effects of Navier-Stokes acceleration to be negligible ($a_i^{(n)} \approx 0$) and resulting equation is,

$$\frac{\Delta \mathcal{E}_k}{\Delta t} = \frac{1}{2} b_i^{(n)} b_i^{(n)} \Delta t + u_i^{(n)} b_i^{(n)} . \tag{3.5}$$

This shows that, in the limit Δt tends to zero the power contribution from spatial force-force term goes to zero and is bounded.

3.1.2 Temporal Correlation of Force

To emphasize and for simplicity consider the sole effect of force on a fluid element (thus Navier-Stokes accelerations are ignored). Force b_i causes an acceleration of the fluid element given by,

$$\frac{\partial u_i(\vec{x}, t)}{\partial t} = b_i(\vec{x}, t) . \tag{3.6}$$

Solving equation (3.6) yeilds,

$$u_i(\vec{x}, t) = \int_{t_0}^{t} b_i(\vec{x}, \tau) d\tau + u_i(\vec{x}, t_0) . \tag{3.7}$$

Where t_0 is some point in time when velocity $u_i(\vec{x}, t_0)$ is known.

We can define integrated kinetic energy as $\langle \mathcal{E}_k \rangle_\ell (t) = \frac{1}{2} \langle u_i u_i \rangle_\ell$. Power input, $\mathcal{P}(t)$ is the rate of change of integrated kinetic energy. Differentiating $\langle \mathcal{E}_k \rangle_\ell (t)$ with respect to t yields,

$$\frac{d \langle \mathcal{E}_k \rangle_\ell (t)}{dt} = \langle u_i b_i \rangle_\ell = \int_{t_0}^{t} \langle b_i(t) b_i(\tau) \rangle_\ell \, d\tau + \langle b_i(t) b_i(t_0) \rangle_\ell . \tag{3.8}$$

22

Thus power input is,

$$\mathcal{P}(t) = \frac{d}{dt}\left\langle\langle\mathcal{E}_k\rangle_\ell\right\rangle_\infty = \int_{t_0}^t \left\langle\langle b_i(t)b_i(\tau)\rangle_\ell\right\rangle_\infty d\tau + \left\langle\langle b_i(t)b_i(t_0)\rangle_\ell\right\rangle_\infty ,$$ (3.9)

where $\langle\cdots\rangle_\infty$ represents ensemble averages over infinite number of realizations. The last term of the above equation shows that temporal force-force correlation contributes to power input and must be accounted for.

The forcing scheme developed by Alvelius uses a force that injects power solely through the fictitious force-force correlation. From equation (3.9) it becomes clear that temporal correlation of this force must be accounted for. For the same, Alvelius employs stochastic processes to ensure that temporal correlation of this force is limited only to the discrete instant in time it exists. In other words, $\left\langle\langle b_i(t)b_i(t_0)\rangle_\ell\right\rangle_\infty$ term in equation (3.9) is set to zero by using stochastic processes.

3.1.3   Various Contributions to Power by Discrete Force

A force in general can be decomposed into components that are perpendicular to the velocity, parallel-in-phase and parallel-out-of-phase with velocity. Consider the Fourier transform of discrete momentum equation (3.2) in all three directions

$$\hat{u}_i^{(n+1)}(\vec{\kappa}) = \hat{u}_i^{(n)}(\vec{\kappa}) + \left(\hat{a}_i^{(n)}(\vec{\kappa}) + \hat{b}_i^{(n)}(\vec{\kappa})\right)\Delta t .$$ (3.10)

$\vec{\kappa}$ is the wave vector and hat $(\hat{\cdot})$ signifies the three dimensional Fourier transform of the quantity. In order to avoid cumbersome notation, for the moment, let the dependence on $\vec{\kappa}$ be dropped. Before steady-state is attained the momentum equation is driven largely by the force term rather than the Navier-Stoke's acceleration terms. Thus, $\hat{a}_i^{(n)}\Delta t$ is assumed to be negligible and ignored. The rate of change of kinetic energy due to the forcing is

$$\frac{\Delta \hat{E}_k}{\Delta t} = \frac{1}{\Delta t} \left(\frac{1}{2} \hat{u}_i^{(n+1)} \hat{u}_i^{(n+1)*} - \frac{1}{2} \hat{u}_i^{(n)} \hat{u}_i^{(n)*} \right) \tag{3.11}$$

$$= \frac{\Delta t}{2} \hat{b}_i^{(n)} \hat{b}_i^{(n)*} + \frac{1}{2} \left(\hat{u}_i^{(n)} \hat{b}_i^{(n)*} + \hat{u}_i^{(n)*} \hat{b}_i^{(n)} \right) ,$$

where asterisk, $(\hat{\cdot})^*$ denotes complex conjugate. The $\hat{b}_i^{(n)} \hat{b}_i^{(n)*} \Delta t/2$ term arises as a result of force being constant over the discrete interval of time Δt. Let the phase and orientation describe the nature of the force. $\hat{b}_i$ can be decomposed into forces that are parallel-in-phase, parallel-out-of-phase and perpendicular with respect to velocity. The contribution to power by these forces respectively are $\hat{P}_1(\vec{\kappa})$, $\hat{P}_2(\vec{\kappa})$, and $\hat{P}_3(\vec{\kappa})$. Observing equation (2.20), in the continuous time formulation, energy is added to the flow only by the component of force parallel-in-phase with velocity. Whereas in discrete time, existence of $\hat{b}_i^{(n)} \hat{b}_i^{(n)*}$ term allows force components parallel-out-of-phase and perpendicular to velocity to add energy. This can be expressed mathematically as,

$$\frac{\Delta \hat{E}_k(\vec{\kappa})}{\Delta t} = \hat{P}_1(\vec{\kappa}) + \hat{P}_2(\vec{\kappa}) + \hat{P}_3(\vec{\kappa}) \tag{3.12}$$

$$= \hat{P}(\vec{\kappa}) .$$

The above equation represents power input at a discrete instant in time.

3.2 Implementing Forcing

Implementing a specific forcing scheme requires three addition steps. The first step is to impose constraints on the force direction and phase. This determines the contributions of $\hat{P}_1$, $\hat{P}_2$ and $\hat{P}_3$ to the forcing spectrum. In most schemes, the only constraint is that the force should not result in a divergent velocity field. Alvelius [1999] shows how to choose a force with an additional constraint being that the force is uncorrelated with the velocity field. Second, the left hand side (LHS) of equation (3.12) must be chosen. In many schemes, equation (3.12) is averaged over wave number bands so that it is in terms of discrete power spectra. Then the LHS is the spectrum of the input

power, hereafter referred to as the "forcing spectrum." For instance, in the scheme of Overholt and Pope [1998] the forcing spectrum is determined by solving differential equations for each wave number band to optimally converge the simulation to a model power spectrum. In the scheme of Alvelius [1999], the forcing spectrum is a Gaussian centered at a specific wave number and invariant in time. The third step in developing a forcing scheme is to combine the previous two steps into a practical algorithm

3.2.1 Constructing a Horizontally-Homogeneous and Isotropic Force

To develop a forcing scheme that is horizontally-homogeneous and isotropic, consider a horizontal force, $\hat{h}_i(\vec{\kappa})$, invariant in the vertical direction, that is, $\hat{h}_i \equiv 0$ if $\kappa_3 \neq 0$. Here $\vec{\kappa} = (\kappa_1, \kappa_2, \kappa_3)$ is the wave number vector. This force expressed in terms of phase and magnitude is

$$\hat{h}_i(\kappa_1, \kappa_2, 0) = \left|\hat{h}_i(\kappa_1, \kappa_2, 0,)\right|_c e^{i\theta_h} e_i , \tag{3.13}$$

with e_i the unit vector defining the direction, $|\cdots|_c$ denoting the magnitude of a complex number, and θ_h the phase. It can be shown that for a horizontally-homogeneous isotropic force that is non-divergent, the horizontal components of the force have the same phase θ_h (refer appendix F). The force is applied for the duration of time step n, but the superscript indicating the time step number is omitted to avoid cumbersome notation.

The complex velocity in the plane $\kappa_3 = 0$ can be expressed similarly as

$$\hat{u}_i(\kappa_1, \kappa_2, 0) = |\hat{u}_i(\kappa_1, \kappa_2, 0)|_c e^{i\theta_u} e_i , \tag{3.14}$$

where θ_u is the phase of velocity. From continuity, $\kappa_1 e_1 + \kappa_2 e_2 = 0$ so that $e_i = (-\kappa_2, \kappa_1)/\kappa_h$ where $\kappa_h = (\kappa_1^2 + \kappa_2^2)^{1/2}$. The constraint that the force not cause divergence in the velocity field requires that the force and velocity be parallel and so e_i in equations (3.13) and (3.14) must be the same vector.

Next, so that the force is horizontally-homogeneous, denote an integral over a circle of radius κ_h by $\oint (\ )d\mathcal{S}(\kappa_h)$, and define

$$U(\kappa_h) = \oint (|\hat{u}_i(\kappa_1, \kappa_2, 0)|_c)d\mathcal{S}(\kappa_h) \ ,$$

$$H(\kappa_h) = \oint (\left|\hat{h}_i(\kappa_1, \kappa_2, 0)\right|_c)d\mathcal{S}(\kappa_h) \ ,$$

and

$$P(\kappa_h) = \oint \hat{P}(\kappa_1, \kappa_2, 0)d\mathcal{S}(\kappa_h) \ .$$

The latter is simply the forcing spectrum from equation (3.12). In terms of the velocity and the horizontal force spectra,

$$\begin{aligned} P(\kappa_h) &= \frac{\Delta t}{2}H^2(\kappa_h) + H(\kappa_h)U(\kappa_h)\frac{\left(e^{i(\theta_h - \theta_u)} + e^{-i(\theta_h - \theta_u)}\right)}{2} \\ &= \frac{\Delta t}{2}H^2(\kappa_h) + H(\kappa_h)U(\kappa_h)\cos(\theta_h - \theta_u) \ , \end{aligned} \tag{3.15}$$

which is a quadratic equation in $H(\kappa_h)$. Given a forcing spectrum, $P(\kappa_h)$, $H(\kappa_h)$ is now defined. Furthermore, we have arrived at the comforting result that for the force, h_i, to be real, $P(\kappa_h)$ must be non-negative (refer section 3.2.2). The first term on the RHS of equation (3.15) corresponds to the power input due to the spatial force-force correlation at a given discrete time-step. That is, it is the horizontal spectrum corresponding to $\hat{P}_1$, which arises from the discretization of time in a simulation. The second term is due to the force-velocity correlation and corresponds to $\hat{P}_2$. A term corresponding to $\hat{P}_3$ cannot occur in this forcing scheme because of the requirement that in 2D the force be parallel to the velocity in order to avoid forcing the flow to be divergent.

Equation (3.15) provides the magnitude of the force that will add to the flow power with spectrum $P(\kappa_h)$. It remains to select the phase of the force. In general, θ_h is a free parameter that can be selected, e.g., stochastically. In this research, the limiting cases of the force and velocity

being exactly in phase or out of phase are considered, and their magnitudes are denoted $F(\kappa_h)$ and $G(\kappa_h)$ that satisfy the equations

$$P(\kappa_h) = \frac{\Delta t}{2}F^2(\kappa_h) + F(\kappa_h)U(\kappa_h) \, , \tag{3.16}$$

$$P(\kappa_h) = \frac{\Delta t}{2}G^2(\kappa_h) \, . \tag{3.17}$$

The force magnitudes have been defined as functions of κ_h. The force can be a function of the local wave number components, κ_1 and κ_2, and so there remains a free parameter in the description of the force, namely the distribution of the force among all the nodes with horizontal wave number magnitude $\kappa_h - \Delta\kappa_h \le \kappa_h < \kappa_h + \Delta\kappa_h$ where $\Delta\kappa_h$ defines the size of a wave number band. In this paper, entirely different approaches are used for choosing this free parameter for the in-phase force than for the out-of-phase force. For the former, it is reasoned that force is applied by amplifying the velocity magnitude and so is inherently distributed across the wave number band. It could be distributed a different way, but a physical justification for doing so is not clear and we choose not to. Therefore

$$\hat{f}_i(\kappa_1, \kappa_2, 0) = F(\kappa_h)e^{i\theta_u}e_i \, . \tag{3.18}$$

The out-of-phase force arises entirely from the discretization of time and, therefore, it has no physical analog. It is inherently uncorrelated with the velocity. As shown by Alvelius, it can also be made uncorrelated with itself in time, such that from equation (3.7) its correlation in time will have the property,

$$\langle g_i(t)g_i(\tau)\rangle_\infty = \mathcal{P}\delta(t - \tau) \, . \tag{3.19}$$

Where, as mentioned earlier $\langle\cdots\rangle_\infty$ represents ensemble averaging over infinite number of realizations,

$$\mathcal{P} = \int\limits_{\kappa_h=\kappa_{min}}^{\kappa_h=\kappa_{max}} P(\kappa_h)d\kappa_h \, . \tag{3.20}$$

27

is the total power injected and κ_{min} and κ_{max} are the maximum and minimum horizontal wave-numbers which indicate the domain of the simulation. Using equation (3.19) in equation (3.9) we can conclude on an average only force-force correlation contributes to the power input,

$$\mathcal{P} = \frac{d}{dt} \langle \mathcal{E}_k \rangle_\infty = \int_{t_n}^{t} \langle \langle b_i(t) b_i(\tau) \rangle_\ell \rangle_\infty d\tau . \tag{3.21}$$

This is possible if the force is stochastically directed among the modes in the wave number band. To achieve this, $G(\kappa_h)$ is replaced by $A(\kappa_h) B(\kappa_1, \kappa_2)$ with $B(\kappa_1, \kappa_2)$ a real random variable uniform in $[0...1]$ and $A(\kappa_h)$ defined by

$$A^2(\kappa_h) = \frac{G^2(\kappa_h)}{\oint B^2(\kappa_1, \kappa_2) d\mathcal{S}(\kappa_h)} . \tag{3.22}$$

Thus, the out-of-phase force is

$$\hat{g}_i(\kappa_1, \kappa_2, 0) = A(\kappa_h) B(\kappa_1, \kappa_2) e^{i\theta_u + \pi/2} e_i . \tag{3.23}$$

3.2.2 Selection of Forcing Spectrum

In section 3.2.1, it is shown how to construct forces that will yield a given forcing spectrum, $P(\kappa_h, t)$. Here, the dependence of the forcing spectrum on time is explicitly shown. As reviewed in section 1.1, quite a few approaches have been used in the past to prescribe the forcing spectrum for turbulence that is homogeneous and isotropic turbulence in all three directions. Here two methods are presented for specifying $P(\kappa_h, t)$. The first method is based on that of Lindborg [2006] and results in constant input power. The forcing spectrum, denoted $Q(\kappa_h)$, is Gaussian centered around forcing wave number, κ_f, and with characteristic width, c:

$$Q(\kappa_h) = C \exp\left[-\left(\frac{\kappa_h - \kappa_f}{c} \right)^2 \right] . \tag{3.24}$$

The constant C determines the total input power.

The second method for specifying $P(\kappa_h, t)$ is based on that of Overholt and Pope [1998]. The resulting spectrum is denoted $R(\kappa_h, t)$. Let $E_k(\kappa_h, t)$ be the horizontally averaged kinetic energy spectrum of the flow at time t and let $E_m(\kappa_h)$ be the target spectrum, that is, the desired $E_k(\kappa_h, t)$ when the simulation is statistically steady. In a simulation with forcing, the spectrum evolves in time according to

$$\frac{\partial E_k(\kappa_h, t)}{\partial t} = R(\kappa_h, t) + \Lambda(\kappa_h, t) \, ,$$

where $\Lambda(\kappa_h)$ accounts for all of the terms in the Navier-Stokes equations except for forcing. For the horizontally-homogeneous isotropic flow scenario, only the horizontal components of velocity with $\kappa_3 = 0$ are forced. Thus,

$$E_f(\kappa_h, t) = \tfrac{1}{2} \oint (\hat{u}_i(\kappa_1, \kappa_2, 0)\hat{u}_i^*(\kappa_1, \kappa_2, 0)) d\mathcal{S}(\kappa_h)$$

(3.25)

$$\text{for } i = 1, 2$$

is the part of kinetic energy spectrum directly affected by forcing. The goal is to determine $R(\kappa_h, t)$ as a function of time that will optimally converge $E_f(\kappa_h, t)$ to $E_m(\kappa_h)$. Letting $E_f(t)$, $R(t)$, and E_m be shorthand notation for $E_f(\kappa_h, t)$, $R(\kappa_h, t)$, and $E_m(\kappa_h)$, respectively, and using dots to indicate differentiation in time,

$$\ddot{E}_f(t) = -\beta \dot{E}_f(t) - \omega_0^2 [E_f(t) - E_m]$$

(3.26)

is an ordinary differential equation for a specific value of κ_h with β the damping coefficient and ω_0 is the angular frequency at which the solution oscillates. Assuming that the forcing dominates the Navier-Stokes terms until the simulation is nearly converged suggests writing equation (3.26) with

$\dot{E}_f(t) = R(t)$. Note that equation (3.26) is critically damped when $\beta = 2\omega_0$. Upon introducing a dimensionless damping factor α, equation (3.26) can be written as,

$$\dot{R}(t) = -2\alpha\omega_0 R(t) - \omega_0^2 [E_f(t) - E_m] \,. \tag{3.27}$$

An under damped, critically damped, and over damped system results when $\alpha < 1$, $\alpha = 1$, and $\alpha > 1$, respectively. The time scale for $R(t)$ to converge to the stationary solution is $\tau = 2\pi/\omega_0$. Letting τ_s be the smallest time scale in the flow then

$$T_f = \frac{\tau}{\tau_s} \tag{3.28}$$

is the ratio of the response time for the forcing to the response time of the turbulence. Thus, α and T_f are simulation parameters that can be tuned to optimize the convergence characteristics of the simulation.

Equation (3.27) does not impose any constraint on the sign of R. Recall from section 3.2.1 that for the the force magnitude to be real requires that $P(\kappa_h)$ be non-negative. This requirement is straightforward to enforce in a simulation simply by setting the force to zero if $R(\kappa_h) < 0$ as is done by Overholt and Pope [1998].

Lastly, it may be desirable to force only some wave numbers, say those below some cutoff value κ_R. In the simulations reported in this paper, setting $R(\kappa_h) = 0$ for $\kappa_h > \kappa_R$ is found to be satisfactory. In other applications, it might be necessary to multiply $R(\kappa_h)$ by a cutoff function such as $\tanh(\kappa_h/\kappa_R)$ (c.f. Ref. Overholt and Pope [1998]).

3.2.3 Specific Forcing Schemes

In section 3.2.1 and 3.2.2, the problem of specifying a scheme for horizontally homogeneous and isotropic forcing was abstracted into the two problems of prescribing the forcing spectrum,

$P(\kappa_h)$, and specifying a force having the desired characteristics and that produces $P(\kappa_h)$. There are endless ways of prescribing the spectrum and specifying the force and so, for specificity, we consider two forces, $\vec{f}$ and $\vec{g}$, and two spectra, Q and R. Of the four possible combinations of force and spectrum schemes, we consider three:

Qf: A constant power scheme with force and velocity in phase.

Qg: A constant power scheme with force and velocity exactly out of phase.

Rf: A constant energy scheme with force and velocity in phase.

All of the schemes force only wave number modes with $\kappa_3 = 0$. As noted by Lindborg [2006], however, it is desirable to excite a small vertical shear when simulating horizontally homogeneous stratified turbulence. To accomplish this, the forcing spectrum is scaled down and a small amount of power is added to the three wave number modes $(0, 0, 3\kappa_m)$, $(0, 0, 4\kappa_m)$, and $(0, 0, 5\kappa_m)$, where κ_m is the smallest non-zero vertical wave number in the simulation. Following Lindborg, 1% of the forcing power is applied to these three modes and the remaining 99% is distributed across the $\kappa_3 = 0$ plane by the forcing scheme.

CHAPTER 4

SIMULATIONS

The characteristics of the three forcing schemes introduced in section 3.2.3 are studied by implementing them in large eddy simulations. The simulated flow is a solution to the Navier-Stokes equations with the Boussinesq assumption and hyperviscous and hyperdiffusion terms replacing the Stokes viscosity and Fick diffusion terms to represent dynamics at scales smaller than the grid spacing. A force term is included in the momentum equation to implement schemes Qf, Qg, or Rf. The thermal energy equation is written in terms of density, and a mean density gradient, $d \langle \tilde{\rho} \rangle_h / dz$, is imposed, with $\langle \cdots \rangle_h$ denoting the planar mean.

4.1   Governing Equations

The governing equations are written in non-dimensional form in terms of characteristic velocity, length, and density scales, $\mathcal{U}$, $\mathcal{L}$, and $\breve{\rho}$, respectively. Note that $\mathcal{U}$ is a characteristic value, not the specific value from any particular simulation. Similarly, $\mathcal{L}$ is a characteristic value since, for each of the forcing schemes, the force is applied over a range of length scales. In terms of these scaling parameters the governing equations are

$$\frac{\partial \breve{u}_i}{\partial \breve{x}_i} = 0 \, , \tag{4.1a}$$

$$\frac{\partial \breve{\rho}}{\partial \breve{t}} + \breve{u}_i \frac{\partial \breve{\rho}}{\partial \breve{x}_i} - \breve{u}_3 = \frac{1}{\breve{\mathrm{Pr}}\breve{\mathrm{Re}}_\ell} \frac{\partial^4 \breve{\rho}}{\partial \breve{x}_i^4} \, , \tag{4.1b}$$

$$\frac{\partial \breve{u}_i}{\partial \breve{t}} + \breve{u}_j \frac{\partial \breve{u}_i}{\partial \breve{x}_j} = -\frac{1}{\breve{\mathrm{F}}_h}\left(\breve{\rho}\delta_{i3}\right) - \frac{\partial \breve{p}}{\partial \breve{x}_i}$$
$$+ \frac{1}{\breve{\mathrm{Re}}_\ell}\left(\frac{\partial^4 \breve{u}_i}{\partial \breve{x}_j{}^4}\right) + \breve{b}_i \,, \tag{4.1c}$$

where, $\breve{\ }$ indicates non-dimensionalized quantities. The hyper-viscous Reynolds, Froude, and tur-
bulent Prandtl numbers are defined as

$$\breve{\mathrm{F}}_h = \frac{\mathcal{U}}{N\mathcal{L}} \,, \quad \breve{\mathrm{Re}}_\ell = \frac{\mathcal{U}\mathcal{L}}{\nu_h} \,, \quad \breve{\mathrm{Pr}} = \frac{\nu_h}{D_h} \,.$$

Here, ν_h is the constant hyper-viscosity and D_h is the constant hyper-diffusivity, g is the mag-
nitude of the gravitational acceleration and $N = \left(-(g/\rho_0)(d\left\langle\tilde{\rho}\right\rangle_h/dz)\right)^{1/2}$ is the Brunt Väisälä
frequency. $\vec{\breve{u}}$ is the velocity vector, $\breve{\rho}$ and $\breve{p}$ are the density and pressure deviations from their hy-
drostatic values. The pressure has been scaled by the dynamic pressure, $\rho_0 \mathcal{U}^2$, and the density by
$\mathcal{L}\left|d\left\langle\tilde{\rho}\right\rangle_h/dz\right|$.

A pseudo-spectral technique is used to compute the spatial derivatives and a third-order Adams-
Bashforth scheme with projection is used to advance the solution in time. A spherical wave-number
truncation of approximately $15/16\,\breve{\kappa}_{max}$, with $\breve{\kappa}_{max}$ the maximum wave number in the discrete
Fourier transforms, is used to reduce aliasing errors. The momentum equation is advanced in
time with the nonlinear term expressed in vorticity form, while the alternating time-step scheme
suggested by Kerr [1985] is employed for the density field to approximate the skew-symmetric
form of the non-linear term and thereby minimize aliasing [Boyd, 2001].

4.2   Simulation Parameters

The simulation parameters can be divided into three groups: those common to all the simula-
tions, those relevant to forcing schemes Qf and Qg, and those relevant to scheme Rf. The common
parameters, listed in Table 4.1, define the size of the computational domain, the (uniform) grid

Table 4.1. Simulation parameters common to all three forcing schemes

$\breve{\mathcal{L}}_h = \mathcal{L}_h/\mathcal{L}$	4
$\breve{\mathcal{L}}_v = \mathcal{L}_v/\mathcal{L}$	0.5
N_h	256 grid points
N_z	32 grid points
$\breve{F}_h$	6.17×10^{-2}
$\breve{Re}_\ell$	7.15×10^{12}
$\breve{Pr}$	1.0

Table 4.2. Simulation parameters for forcing scheme Qf and Qg

$\breve{\kappa}_f$	4.0
$\breve{c}$	3.0
$\breve{\mathcal{P}}$	1.0

Table 4.3. Simulation parameters for forcing scheme Rf

$\breve{\alpha}$	1.8
$\breve{\kappa}_R$	10
$\breve{T}_f$	0.4

spacing, and the physical parameters not associated with forcing. In the table, $\breve{\mathcal{L}}_h$ and $\breve{\mathcal{L}}_v$ are, respectively, the horizontal and vertical dimensions of the three-dimensional computational domain, and N_h and N_z are the corresponding number of grid points. For all the simulations, the velocity fields are initialized to zero everywhere, as is the deviatoric density, $\breve{\rho}$.

In the constant power forcing schemes, Qf and Qg, three independent parameters define the forcing scheme. It is convenient to choose these to be the forcing power, $\breve{\mathcal{P}}$ and the mean, $\breve{\kappa}_f$, and variance, $\breve{c}$, of $\breve{Q}(\breve{\kappa}_h)$. The peak value of that function, $\breve{C}$, is then defined by (c.f. equation (3.24))

$$\breve{C} = \frac{\breve{\mathcal{P}}}{\displaystyle\int_{\breve{\kappa}_{min}}^{\breve{\kappa}_{max}} \exp\left[-\left(\frac{\breve{\kappa}_h - \breve{\kappa}_f}{\breve{c}}\right)^2\right] d\breve{\kappa}_h} . \tag{4.2}$$

where $\breve{\kappa}_{min}$ is the minimum wave number in the discrete Fourier transforms. In terms of the characteristic velocity and length scales, $\breve{\mathcal{P}} = \mathcal{P}/(\mathcal{U}^3/\mathcal{L})$ and $\breve{\kappa}_f = 2\pi/\mathcal{L}$. The parameters for the Qf and Qg simulations are given in Table 4.2. Simulation Qg corresponds exactly to Lindborg's run 1.

The parameters specific to forcing scheme Rf are the target energy spectrum $\breve{E}_m(\breve{\kappa}_h)$, the highest wave number forced, $\breve{\kappa}_R$, the damping coefficient, $\breve{\alpha}$, and the forcing time scale ratio, $\breve{T}_f$. $\breve{E}_m(\breve{\kappa}_h)$ is set equal to the stationary solution from case Qf so that the characteristics of the different forcing schemes can be easily compared. The remaining parameters are as shown in Table 4.3. These were determined by trial and error. Most interesting is the behavior of the scheme for different values of $\breve{\alpha}$. Let $\breve{\mathcal{E}}_f(\breve{t})$ be the total horizontal kinetic energy in all the wave numbers being forced and $\breve{\mathcal{E}}_m$ the corresponding target value. The ratio $\breve{\mathcal{E}}_f(\breve{t})/\breve{\mathcal{E}}_m$ is plotted versus time in figure 4.1. When equation (3.27) is under damped ($\breve{\alpha} = 0.4$) or critically damped ($\breve{\alpha} = 1.0$) then there is significant oscillation of the energy about the target value. When equation (3.27) is over damped ($\breve{\alpha} = 1.8$) then the energy converges to the target nearly optimally. This result is consistent with those of Overholt and Pope. Of course convergence of $\breve{\mathcal{E}}_f(\breve{t})/\breve{\mathcal{E}}_m$ to unity does not ensure convergence of the spectrum to the target spectrum at each wave number, but this was the case in our simulations.
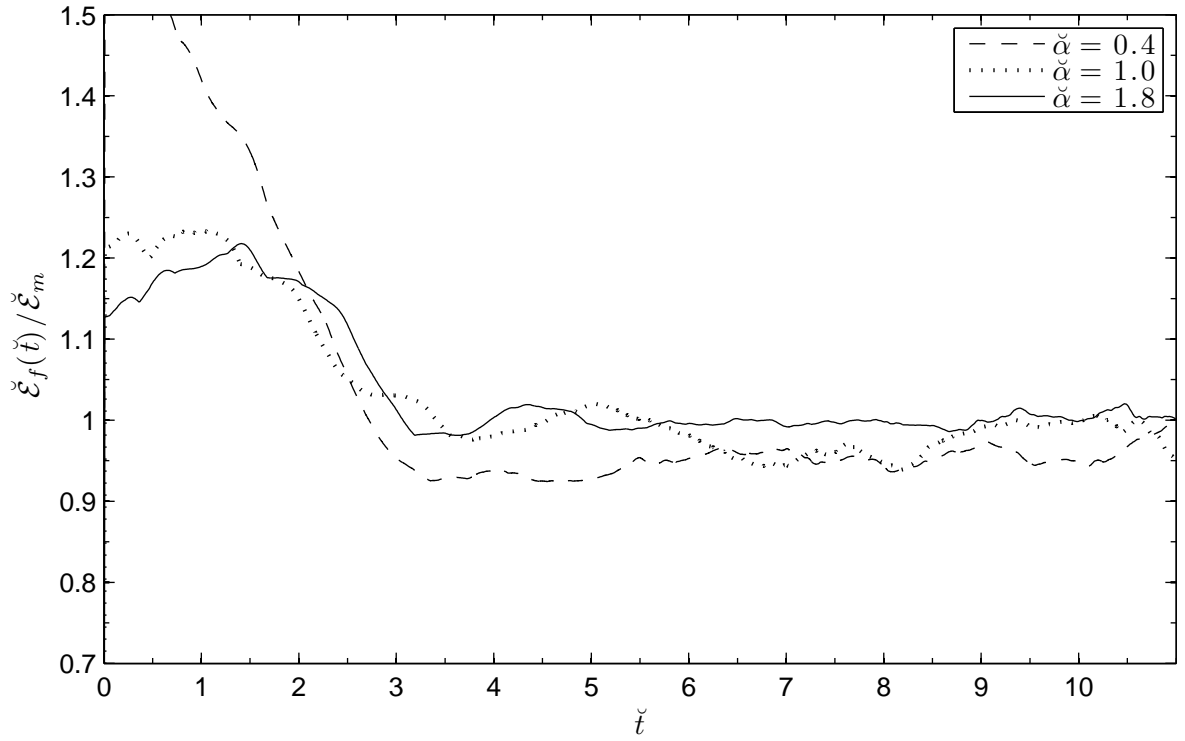
Figure 4.1. Time evolution of the ratio of horizontal contribution to kinetic energy at the forcing plane to target energy for scheme Rf.

CHAPTER 5

RESULTS

Analysis of the simulation results is divided into three sections. First it is verified that the prescribed input power for the Q schemes, and the prescribed model spectrum for the R scheme, are achieved. Second, the performance of the schemes are evaluated in terms of the time it takes for the solution to converge and the overshoot in kinetic energy. Third, some characteristics of schemes are examined in terms of the physical phenomenon that they are designed to emulate.

5.1 Verification

The most important characteristic of a forcing scheme is that the numerical implementation applies the desired force. This may seem like a matter of accurately writing the software, but in light of the insight by Alvelius that the discretized transport equations allow for power inputs that have no analog in the continuous equations, it is worthwhile to verify that the careful theoretical development in chapter 3 does indeed carry over to the actual simulations. This has been done for the simulations by verifying that the power input by force-force and force-velocity correlations are as prescribed, that the desired forcing or target spectra result, and that the statistics of the steady-state solutions are independent of the size of the time step in the simulations.

In this paper, demonstration of the numerical implementations is limited to showing that the prescribed power or prescribed model spectrum is achieved. These are shown in figure 5.1 and 5.2. In figure 5.1 it is evident that the time-averaged forcing spectrum, $\overline{\breve{\mathcal{P}}}(\breve{\kappa}_h)$, matches that specified by equation (3.24). The over bar denotes time averaging over a period of about one large eddy turn
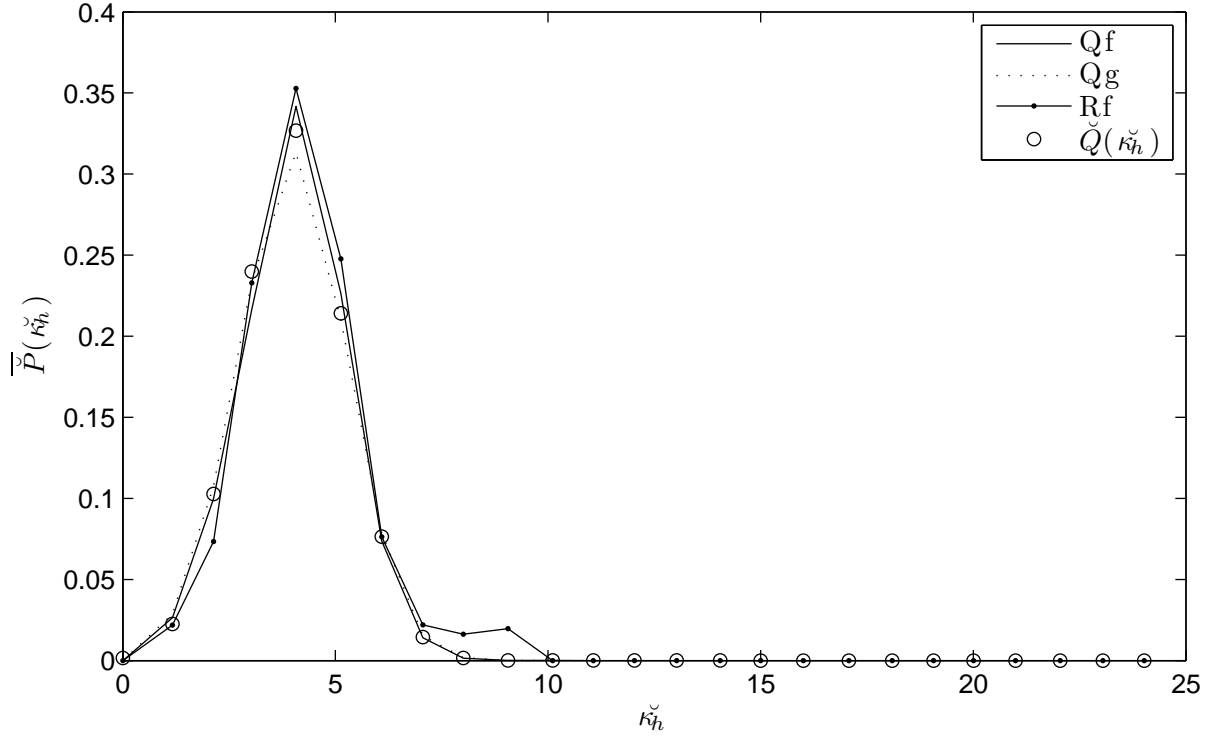
Figure 5.1. The agreement between forcing spectrum defined by equation (3.24) and actual injected forcing spectrum for the Qf and Qg schemes.

over time, that is, over unity dimensionless time. Also included in the plot is the spectrum of the input power in the Rf scheme.

Figure 5.2 shows the agreement between the target spectrum, $\breve{E}_m$, and the steady-state spectrum for scheme Rf. As with the Q schemes, the implementation yields the desired results. Also shown in the figure are the steady state spectra for the Q schemes. Recall that the model spectrum was chosen to be the converged spectrum from scheme Qf. The spectrum for the Qg scheme should not necessarily agree with the other two. From figures 5.1 and 5.2 and other analyses not shown, it is concluded that the theory from chapter 3 is accurately implemented in the time- and space-discrete simulations.
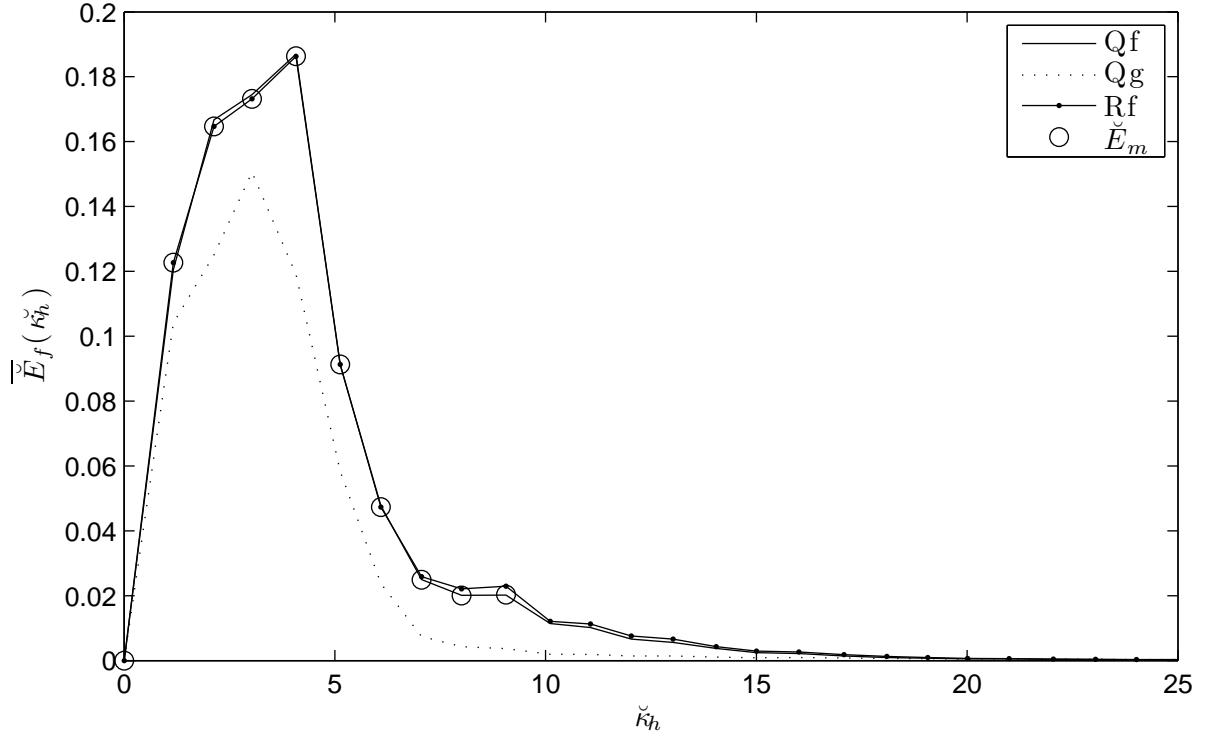
Figure 5.2. The agreement between model spectrum, $\breve{E}_m(\breve{\kappa}_h)$ and $\overline{\breve{E}}_f(\breve{\kappa}_h)$ for the Rf scheme.

A principle difference between the f and g forces is expected in their temporal autocorrelations. Let the autocorrelation of the force, $\breve{\vec{b}}$, be denoted $\left\langle \breve{\vec{b}} \star \breve{\vec{b}} \right\rangle_\ell (\breve{\tau})$ with $\breve{\tau}$ the separation in time and as mentioned earlier, $\langle \cdots \rangle_\ell$ indicates that the correlations have been averaged over space. This quantity is plotted for the three forcing schemes in figure 5.3. As expected from the derivation by Alvelius [1999], the g force is not correlated in time and so the autocorrelation is non-zero only at $\breve{\tau} = 0$. The f force is correlated over a separation time of $\breve{\tau} > 1$. This is consistent with the idea that the f force represents the effects of coherent structures larger than the simulation domain. The correlation time of the f force as implemented in the Rf scheme is slightly less than as in the Qf schemes. This is as expected since the magnitude of the force varies in time with the Rf approach but not with the Qf approach.
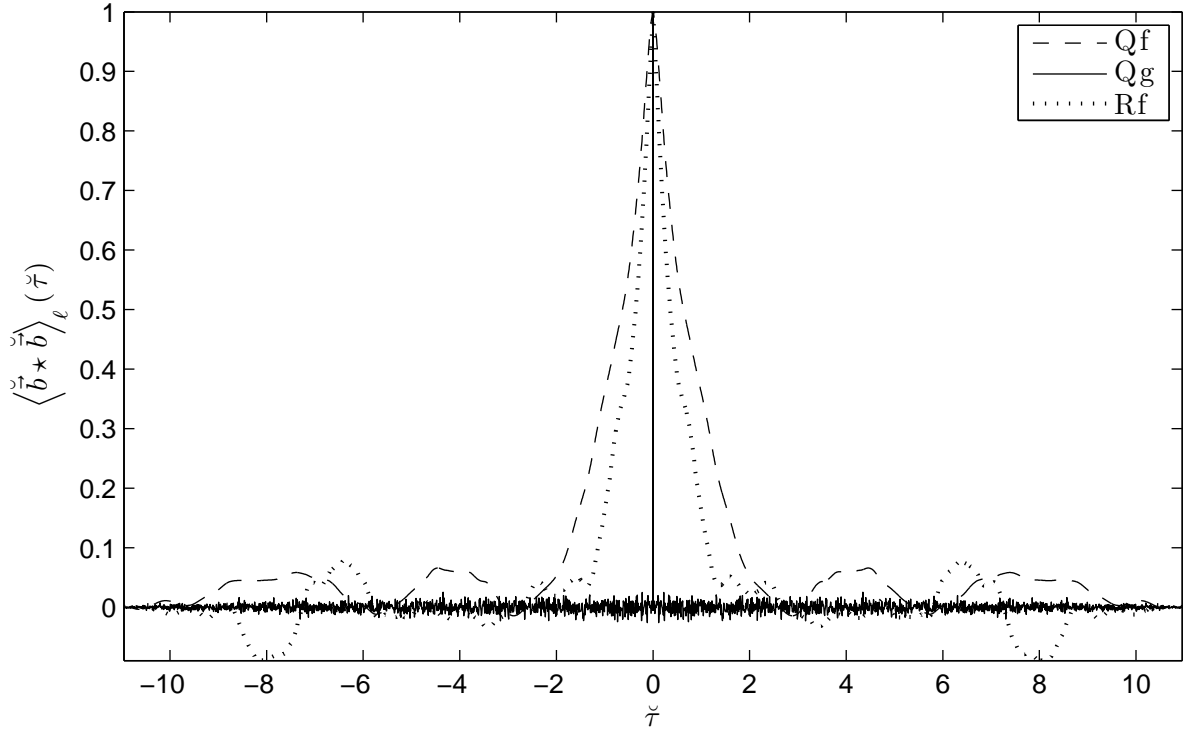
Figure 5.3. The spatially averaged temporal autocorrelation of the force, $\overset{\smallsmile}{\vec{b}}$ for each forcing scheme.

5.2 Performance

An important metric by which to judge the performance of a forcing scheme is the time it takes for the simulation to converge to steady state. Of course the statistics that must be converged, and the criteria by which convergence is judged, are dependent on the purpose of the particular simulation. Here, several flow statistics are considered as functions of time in order to gain an appreciation for the convergence characteristics of the three forcing schemes.

5.2.1 Dissipation Rate and Forcing Power

Given the choice made in chapter 4 to make the domain-averaged forcing power a simulation parameter, a natural test for convergence is that the total energy dissipation rate, that is, the sum
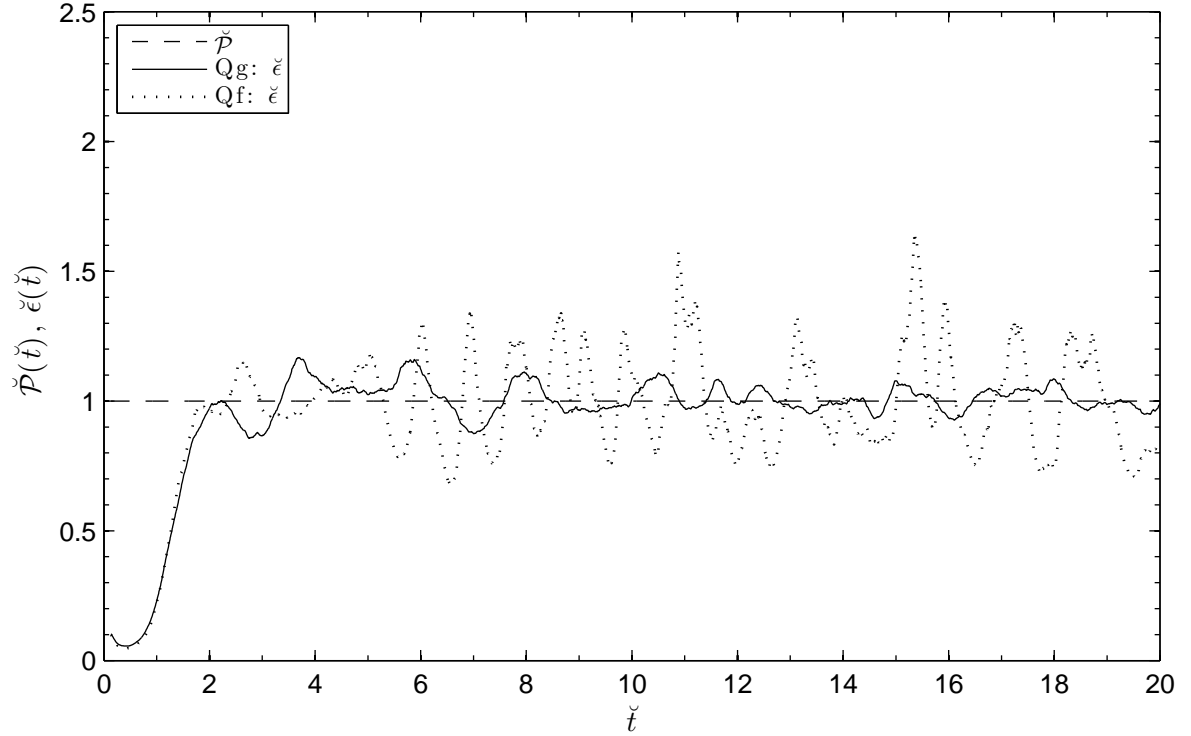
Figure 5.4. Time evolution of spatially averaged energy dissipation rate, $\breve{\epsilon}(\breve{t})$ and forcing power, $\breve{\mathcal{P}}(\breve{t})$ for the Qf and Qg schemes.

of the dissipation rates of kinetic and available potential energy, equals the forcing power when averaged over time. The total dissipation rate is denoted $\breve{\epsilon}(\breve{t}) = \breve{\epsilon}_k(\breve{t}) + \breve{\epsilon}_p(\breve{t})$ and is plotted, along with forcing power in Fig. 5.5. The possibility of time dependent forcing power, as occurs in the Rf scheme, is made explicit with the notation $\breve{\mathcal{P}}(\breve{t})$ even though it is, by definition, constant in the Q schemes.

In all cases, $\breve{\epsilon}(\breve{t})$ and $\breve{\mathcal{P}}(\breve{t})$ converge, to the extent that they ever will, by about $\breve{t} = 2$. This transient is a reflection on the flow physics as much as on the forcing schemes as it takes some time for the gradients responsible for dissipation to develop. It is known that this flow transfers energy down scale [Lindborg, 2006], and the cascade takes time to develop.
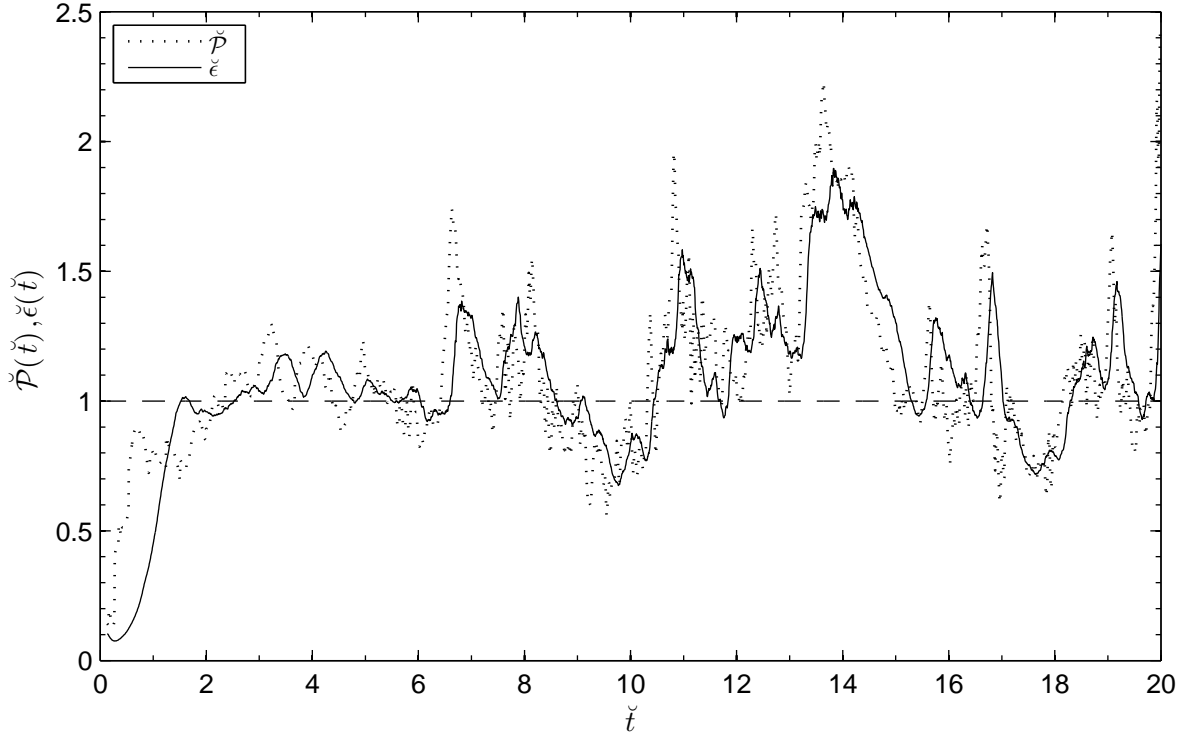
Figure 5.5. Time evolution of spatially averaged energy dissipation rate, $\breve{\epsilon}(\breve{t})$ and forcing power, $\breve{\mathcal{P}}(\breve{t})$ for the Rf scheme.

The oscillation of $\breve{\epsilon}(\breve{t})$ about $\breve{\mathcal{P}}(\breve{t})$ in the Q schemes apparently reflects some interaction between the forcing and the flow physics since the Qf and Qg schemes behave differently. Recall that the Qf scheme is designed with the thought that the forcing represents the effects of length and time scales larger than those in the simulation domain so that the force is correlated with the velocity. In the Qg scheme, the discrete nature of the time-stepping is taken advantage of to add power with the force-velocity correlation zero. The Qg approach has no physical analog but, from Fig. 5.5, it has the potentially useful characteristic that it produces a more nearly constant dissipation rate than does the Qf scheme. With the Rf scheme, the dynamics are even more complicated since both $\breve{\epsilon}(\breve{t})$ and $\breve{\mathcal{P}}(\breve{t})$ are responding to the flow. Significant variations over time of both $\breve{\mathcal{P}}(\breve{t})$ and $\breve{\epsilon}(\breve{t})$ occur.
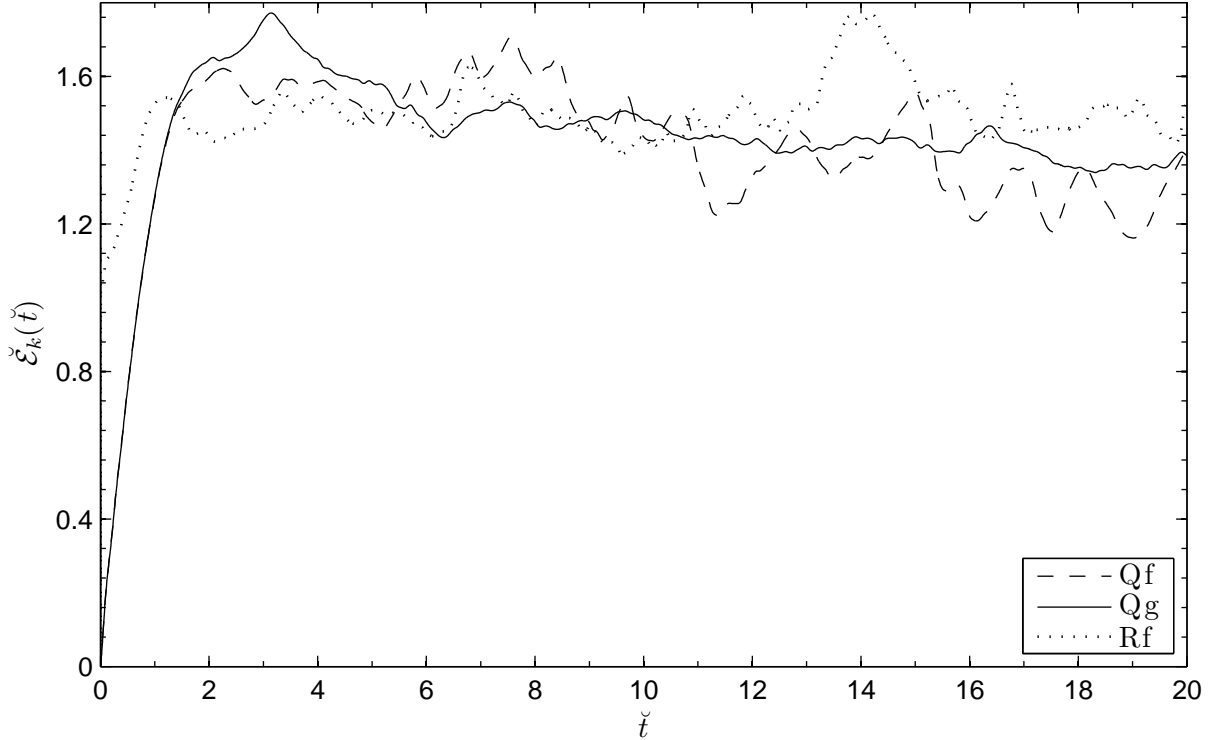
Figure 5.6. Time evolution of the domain-averaged kinetic energy, $\breve{\mathcal{E}}_k(\breve{t})$, for all schemes.

5.2.2 Energy

While the time to convergence of the dissipation rate is about the same for all the schemes since it is dependent on the flow physics, the time required for the kinetic energy to converge depends much more strongly on the forcing scheme. The domain average kinetic energy, $\breve{\mathcal{E}}_k(\breve{t})$, is shown for each scheme in Fig. 5.6. Consistent with the results of Lindborg, the Qg scheme causes the kinetic energy to overshoot and then converge by about $\breve{t} = 20$. The results of the Qf scheme are comparable. The Rf scheme, on the other hand, converges the kinetic energy by about $\breve{t} = 2$.

Recall that the force in all the schemes is applied on the plane $\breve{\kappa}_3 = 0$, except for the very small forces used to induce vertical shear. The energy on the forced plane, $\breve{\mathcal{E}}_f(\breve{t})$, is shown in Fig. 5.7. Here it is very evident that the Rf scheme converges to the target energy with very little deviation
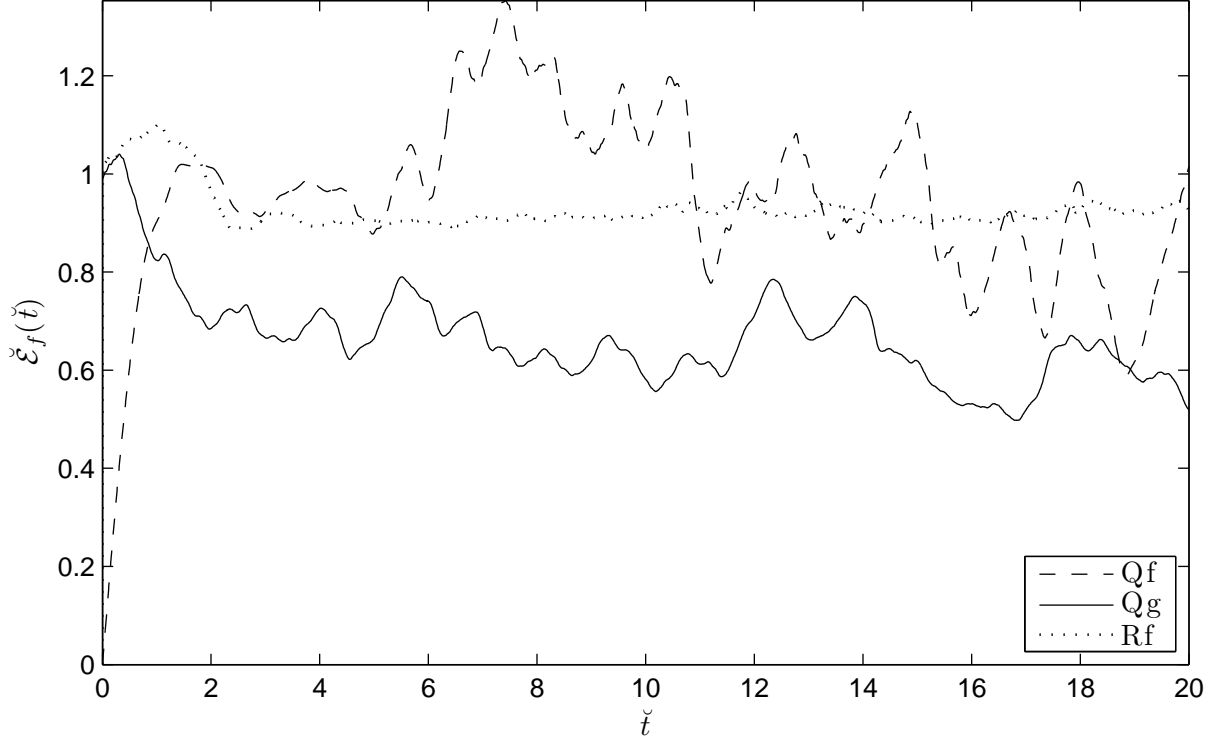
Figure 5.7. Time evolution of kinetic energy in the modes being forced, $\breve{\mathcal{E}}_f(\breve{t})$, for all schemes.

from the time-averaged value after about $\breve{t} = 2$. The target spectrum for the Rf scheme was taken from the converged solution for the Qf scheme and so, as expected, the Qf and Rf schemes converge to the same energy on the forced plane.

As discussed at the beginning of section 1.1, schemes that emulate physical forces are attractive since the simulation results can then be matched to laboratory flows. For the forcing methods presented in this paper, the characteristics of the forces must be deduced from their effects on the simulated flow. Looking again at Figs. 5.6 and 5.7, it is apparent that the Qf and Qg schemes result in comparable time-averaged values of $\breve{\mathcal{E}}_k(\breve{t})$ yet different values of $\breve{\mathcal{E}}_f(\breve{t})$. Evidently, the average $\breve{\mathcal{E}}_k(\breve{t})$ is dominated by the flow physics and so it is not strongly dependent on the details of the forcing while the average $\breve{\mathcal{E}}_f(\breve{t})$ does depend on the exact characteristics of the force.

44

5.3 Conclusions

Forcing schemes that emulate physical flows are attractive since the characteristics of the force are clear in terms of physical processes. Many times, however, it is desirable to use a numerical forcing method that has no physical analog. When this is done, the metrics for judging the forcing scheme are quite subjective as reflected in the considerable discussion in the literature, reviewed in section 1.1. The framework for writing general schemes for applying forces in Fourier space is developed by taking advantage of several decades of work on forcing schemes for isotropic homogeneous turbulence. In this framework, the tasks of choosing the forcing spectrum and choosing the characteristics of the force are abstracted and treated separately. We then use the framework to write several forcing schemes for horizontally homogeneous and isotropic, vertically stratified flows.

An important advance in forcing schemes was made by Alvelius [1999]. He noted that in the time-discretized fluid transport equations, a force does not need a component parallel to and in phase with the velocity in order to add energy. This fact is taken advantage of here to create forces that are either perfectly correlated with or perfectly uncorrelated with the velocity. Additionally, the deterministic forcing scheme of Overholt and Pope [1998] is used as the basis for a fast-converging scheme that may be appropriate in cases when a target steady-state energy spectrum is known.

Three forcing schemes, developed in terms of the new framework, are tested in large-eddy simulations. Each has different characteristics and which is "best" depends on the metrics of interest. The deterministic scheme with the force and velocity correlated, scheme Rf, converges the fastest but the variability in the domain-averaged kinetic energy when the flow is statistically steady is greater than in the other schemes. It also requires a target spectrum to be known *a priori*, which might not be possible when simulating new flow configurations. The least variability in kinetic energy at steady state is observed with scheme Qg in which non-zero forcing power is realized only because of the discrete time stepping and the force is uncorrelated with itself in time.

The underlying bias is that the forcing scheme should represent motions at length and time scales that are large compared with those in the simulation. Scheme Qg is undesirable on this basis, but the resulting low variance in the domain-averaged kinetic energy is attractive.

The results of the three sample schemes demonstrates that the utility of a particular forcing technique is closely coupled with the purpose of the simulations. Using the framework presented to abstract the components of the forcing scheme makes it straightforward to develop a family of schemes for a particular application. Simple test runs then reveal the effects of each forcing method on the simulated flow.

APPENDIX A

STRESS TENSOR

The momentum of a fluid element with infinitesimal volume dV is $\rho_t u_i dV$. The equation for the time rate change of momentum of a material region $\mathcal{M}$ is,

$$\frac{D}{Dt} \left(\int_{\mathcal{M}} \rho_t u_i dV \right) = \int_{\mathcal{M}} \rho_t F_i dV + \int_{\mathcal{M}} R_i dS \; . \tag{A.1}$$

F_i and R_i represent the body forces and surface forces acting on the fluid element respectively. Using Liebnitz and Gauss theorem we can arrive at,

$$\int_{\mathcal{M}} \left[\frac{\partial}{\partial t} \left(\rho_t u_i \right) + \frac{\partial}{\partial x_i} \left(\rho_t u_j u_i \right) \right] dV = \int_{\mathcal{M}} \rho_t F_i dV + \int_{\mathcal{M}} R_i dS \; . \tag{A.2}$$

A.1 Stress Tensor

Let T_{ij} be a stress tensor such that

$$R_j \left(\vec{n}; \vec{x} \right) = n_i T_{ij} \; , \tag{A.3}$$

where n_i is the outward drawn normal to the surface element dS at position $\vec{x}$ [Panton, 1984] . For a stationary fluid the only normal stress that exists is thermodynamic pressure p_t. Thermodynamic pressure is a function of the thermodynamic state of a fluid, that is $p_t : p_t(e, \rho_t)$. However, when a fluid is in motion, viscous stresses (τ_{ij}) exist in addition to p_t to balance the imbalances in force causing motion. Thus

$$T_{ij} = -p_t \delta_{ij} + \tau_{ij} \; . \tag{A.4}$$

A.2 Mechanical and Thermodynamic Pressure

Thermodynamic pressure contributes to normal stress on the surface of a fluid element and it is isotropic. However, when a fluid is in motion normal viscous stresses come into existence and are not isotropic. The average of normal stresses, termed as mechanical pressure (p_m) is used to understand normal surface forces.

$$p_m = -\frac{1}{3}\left(T_{11} + T_{22} + T_{33}\right) = -\frac{1}{3}T_{ii} \ . \tag{A.5}$$

As per Stoke's assumption, the difference in mechanical and thermodynamic pressure is considered to be a linear function of the rate of expansion [Panton, 1984],

$$p_m - p_t = \beta_p \nabla \cdot \vec{u} = -\frac{\beta_p}{\rho_t}\frac{D\rho_t}{Dt} \tag{A.6}$$

where β_p is the bulk modulus. For incompressible fluids β_p is zero and hence there is no difference between p_m and p_t. In other words, Stoke's assumption implies that, the average normal viscous stress is zero.

A.3 Navier-Stokes Stress Tensor

Most fluids are isotropic having no moments on their surfaces thereby implying the stress tensor to be symmetric. Also T_{ij} is assumed to be linearly dependent on velocity gradients. Then T_{ij} can be written as [Aris, 1962; Batchelor, 1956; Prager, 1961; Yih, 1974]

$$T_{ij} = \left(-p_t + \lambda\frac{\partial u_k}{\partial x_k}\right)\delta_{ij} + 2\mu\left(\frac{\partial u_j}{\partial x_i}\right)_{sym} \ . \tag{A.7}$$

Where λ is the second coefficient of viscosity, μ is the first coefficient of viscosity (assumed to be a constant) and $(\partial u_j/\partial x_i)_{sym}$ is the symmetric strain rate tensor, S_{ij}. The symmetric strain rate

tensor is defined as,

$$S_{ij} \equiv \frac{1}{2}\left(\frac{\partial u_i}{\partial x_j} + \frac{\partial u_j}{\partial x_i}\right) = \left(\frac{\partial u_j}{\partial x_i}\right)_{sym} . \tag{A.8}$$

Contracting equation (A.7) on i and dividing by 3 gives,

$$p_t - p_m = \left(\lambda + \frac{2}{3}\mu\right)\frac{\partial u_k}{\partial x_k} = -\left(\lambda + \frac{2}{3}\mu\right)\frac{1}{\rho_t}\frac{D\rho_t}{Dt} . \tag{A.9}$$

Low mach number flows have quick relaxation (time taken for energy be to be equally distributed into rotational, translational and vibrational modes) thus the difference between thermodynamic and mechanical pressure is negligible (Stoke's assumption). Therefore, $\lambda = -\frac{2}{3}\mu$. Substituting for λ in equation (A.7), the final expression for Navier-Stokes stress tensor is obtained,

$$T_{ij} = -p_t\delta_{ij} + \tau_{ij} ,$$
$$= \left(-p_t - \frac{2}{3}\mu\frac{\partial u_k}{\partial x_k}\right)\delta_{ij} + 2\mu S_{ij} . \tag{A.10}$$

The Navier-Stokes viscous stress tensor is,

$$\tau_{ij} = -\frac{2}{3}\mu\frac{\partial u_k}{\partial x_k}\delta_{ij} + 2\mu S_{ij} . \tag{A.11}$$

The momentum equation (2.3) has a $\partial\tau_{ij}/\partial x_j$ term, which for the Navier-Stokes viscous tensor

$$\frac{\partial\tau_{ij}}{\partial x_j} = \frac{1}{3}\mu\frac{\partial}{\partial x_i}\left(\frac{\partial u_j}{\partial x_j}\right) + \mu\frac{\partial^2 u_i}{\partial x_j^2} . \tag{A.12}$$

For an incompressible flow $\partial u_i/\partial x_i = 0$ and assuming μ to be a constant, the above equation simplifies to,

$$\frac{\partial\tau_{ij}}{\partial x_j} = 2\mu\frac{\partial S_{ij}}{\partial x_j} = \mu\frac{\partial^2 u_i}{\partial x_j^2} . \tag{A.13}$$

An important identity to note is that, product of a symmetric tensor with any tensor results in a symmetric tensor, thus

$$S_{ij}\frac{\partial u_i}{\partial x_j} = S_{ij}S_{ij} \ . \tag{A.14}$$

APPENDIX B

INTERNAL ENERGY EQUATION

Internal energy cannot be measured directly but instead it is inferred from temperature. Thus it is beneficial to re-cast equation (2.7) in terms of temperature. Enthalpy per unit mass, h is given as [Panton, 1984],

$$h = e + \frac{p_t}{\rho_t} \ .$$
(B.1)

Equation (2.7) redefined in terms of enthalpy is [Bird et al., 2002],

$$\rho_t \frac{Dh}{Dt} = \frac{\partial}{\partial x_i} \left(k_T \frac{\partial T}{\partial x_i} \right) + \tau_{ij} \frac{\partial u_i}{\partial x_j} + \frac{Dp_t}{Dt} \ .$$
(B.2)

Assuming enthalpy to be a function of only temperature (T) and thermodynamic pressure (p_t), the differential form of equation (B.1) is,

$$dh = \left(\frac{\partial h}{\partial T} \right)_{p_t} dT + \left(\frac{\partial h}{\partial p_t} \right)_T dp_t \ ,$$
(B.3)

where the quantity in the subscript indicates that it is being held constant for the differential at hand. The first term on the right hand side of equation (B.3) is recognized to be the specific heat at constant pressure, C_p and the second term on the right hand side is evaluated using equation (B.1) to give,

$$dh = C_p dT + \frac{1}{\rho_t} \left(1 + T\beta_t \right) dp_t \ ,$$
(B.4)

where $\beta_t \equiv (-1/\rho_t)(\partial \rho_t/\partial T)_{p_t}$ is the coefficient of thermal expansion. Multiplying equation (B.4) with ρ_t and equating it with the right hand side of equation (B.2) gives,

$$\rho_t C_p \frac{DT}{Dt} = \frac{\partial}{\partial x_i}\left(k_T \frac{\partial T}{\partial x_i}\right) + \tau_{ij}\frac{\partial u_i}{\partial x_j} + T\beta_t \frac{Dp_t}{Dt} \; . \tag{B.5}$$

Using scaling analysis shown in Kundu and Cohen [2002] reveals the contribution of viscous stresses to be negligible. Thus the internal energy equation is,

$$\rho_t C_p \frac{DT}{Dt} = \frac{\partial}{\partial x_i}\left(k_T \frac{\partial T}{\partial x_i}\right) + T\beta_t \frac{Dp_t}{Dt} \; . \tag{B.6}$$

APPENDIX C

BOUSSINESQ EQUATIONS

In this section the Boussinesq approximation with a forcing term in the momentum equation is discussed.

C.1 Decomposition of Density and Pressure

Consider a physical variable (ψ_t) decomposed into its spatial average (ψ_o), its variation in absence of motion $(\tilde{\psi})$ and fluctuations due to fluid motion (ψ). [Spiegel and Veronis, 1960]

$$\psi_t(\vec{x}, t) = \psi_o + \tilde{\psi}(z) + \psi(\vec{x}, t) \ . \tag{C.1}$$

ψ_o would be time dependent if boundary conditions vary with time, however for simplicity it is assumed independent of time. The physical quantities of interest are density and pressure and are decomposed as,

$$
\begin{aligned}
\rho_t(\vec{x}, t) &= \rho_0 + \tilde{\rho}(z) + \rho(\vec{x}, t) \ , \\
p_t(\vec{x}, t) &= p_o + \tilde{p}(z) + p(\vec{x}, t) \ .
\end{aligned}
\tag{C.2a}
$$

We can obtain a scale for heights, especially for density as,

$$D_\rho = \left| \frac{\rho_0}{(d\tilde{\rho}/dz)} \right| \ . \tag{C.3}$$

The approximation we wish to make is that the fluid motions are confined to a layer of height d that is much less than the smallest scale height, $D = (D_\rho)_{min} \gg d$. Integrating from the height of minimum density to maximum density $(\tilde{\rho}_{max} - \tilde{\rho}_{min}) = \Delta\tilde{\rho}$, we get and define,

$$\frac{\Delta\tilde{\rho}}{\rho_0} \equiv \varepsilon \ll 1 \,. \tag{C.4}$$

This becomes the static condition that requires to be imposed to make the above approximation. This holds for infinitesimal amplitudes of motion. However, for non-linear analysis we have,

$$\left|\frac{\rho}{\tilde{\rho}}\right| \leq O(\varepsilon) \,. \tag{C.5}$$

This says that the magnitude of fluctuations should not exceed in order of magnitude the static variation. This must be verified *a posteriori* from solutions to the problem.

C.2 Hydrostatic Relation

The momentum equation (2.3) simplified using equation (2.2) with gravity and external forcing being the only body forces is

$$\rho_t \frac{\partial u_i}{\partial t} + \rho_t u_j \frac{\partial u_i}{\partial x_j} = -\frac{\partial p_t}{\partial x_i} + \rho_t \left(-g\delta_{i3} + b_i\right) + \mu \frac{\partial^2 u_i}{\partial x_j^2} + \frac{\mu}{3}\frac{\partial}{\partial x_i}\left(\frac{\partial u_j}{\partial x_j}\right) \,, \tag{C.6}$$

and continuity equation (2.2) is

$$\frac{D\rho_t}{Dt} = -\rho_t \frac{\partial u_i}{\partial x_i} \,. \tag{C.7}$$

In absence of motion and external forcing, equation (C.6) simplifies to,

$$\frac{\partial \tilde{p}}{\partial x_i} = -g\left(\rho_0 + \tilde{\rho}\right)\delta_{i3} \,, \tag{C.8}$$

54

in other words,

$$\frac{d\tilde{p}}{dz} = -g\left(\rho_0 + \tilde{\rho}\right) . \tag{C.9}$$

Equation (C.9) is the hydrostatic relation and is assumed to hold true even when motion exists. Substituting the hydrostatic relation in the momentum equation we obtain,

$$\rho_t \frac{\partial u_i}{\partial t} + \rho_t u_j \frac{\partial u_i}{\partial x_j} = -\frac{\partial p}{\partial x_i} - \rho g \delta_{i3} + \rho_t b_i + \rho_0 \nu \frac{\partial^2 u_i}{\partial x_j^2} + \frac{\rho_0 \nu}{3} \frac{\partial}{\partial x_i} \left(\frac{\partial u_j}{\partial x_j}\right) . \tag{C.10}$$

C.3 The Boussinesq Approximation

The continuity and momentum equation are scaled in factors of $O\left(\varepsilon\right)$. The Taylor's series expansion of $(1/\rho_t)$ in terms of ρ_0 is,

$$\rho_t^{-1} = \rho_0^{-1} - \rho_0^{-2}\left(\rho_t - \rho_0\right) + \rho_0^{-3}\left(\rho_t - \rho_0\right)^2 - \cdots . \tag{C.11}$$

Substituting equation (C.2) gives,

$$\rho_t^{-1} = \rho_0^{-1}\left(1 - \left(\frac{\tilde{\rho}}{\rho_0} + \frac{\rho}{\rho_0}\right) + \left(\frac{\tilde{\rho}}{\rho_0} + \frac{\rho}{\rho_0}\right)^2 - \cdots\right) . \tag{C.12}$$

Noting that $(\tilde{\rho}/\rho_0) \le O\left(\varepsilon\right)$ and $(\rho/\rho_0) \le O\left(\varepsilon\right)$, the above equation is,

$$\frac{1}{\rho_t} = \frac{1}{\rho_0}\left(1 - O\left(\varepsilon\right) + O\left(\varepsilon^2\right) - \cdots\right) . \tag{C.13}$$

C.3.1 Continuity Equation

Substituting equation (C.2) for density in equation (C.7) while taking ρ_0 common gives,

$$\frac{-1}{\rho_t} \frac{D}{Dt}\left[\rho_0\left(1 + \frac{\tilde{\rho}}{\rho_0} + \frac{\rho}{\rho_0}\right)\right] = \frac{\partial u_i}{\partial x_i} . \tag{C.14}$$

Using equations (C.4) , (C.5) and (C.13) in the above equation gives,

$$-\frac{D}{Dt}\left[\varepsilon\frac{\tilde{\rho}}{\Delta\tilde{\rho}} + \varepsilon\frac{\rho}{\Delta\tilde{\rho}}\right] + O\left(\varepsilon^2\right) = \frac{\partial u_i}{\partial x_i} . \tag{C.15}$$

Keeping to the first order, the continuity equation is then,

$$\frac{\partial u_i}{\partial x_i} = 0 . \tag{C.16}$$

C.3.2   Momentum Equation

Similar to the continuity equation, the momentum equation (C.10) after using relation (C.13) and keeping to first order is,

$$\frac{Du_i}{Dt} = -\frac{1}{\rho_0}\frac{\partial p}{\partial x_i} - \frac{\rho}{\rho_0}g\delta_{i3} + b_i + \nu\frac{\partial^2 u_i}{\partial x_j^2} + \frac{\nu}{3}\frac{\partial}{\partial x_i}\left(\frac{\partial u_j}{\partial x_j}\right) . \tag{C.17}$$

Expressing the momentum equation in terms of ε gives,

$$\frac{Du_i}{Dt} = -\frac{\varepsilon}{\Delta\tilde{\rho}}\frac{\partial p}{\partial x_i} - \frac{\varepsilon}{\Delta\tilde{\rho}}g\rho\delta_{i3} + b_i + \nu\frac{\partial^2 u_i}{\partial x_j^2} + \frac{\nu}{3}\frac{\partial}{\partial x_i}\left(\frac{\partial u_j}{\partial x_j}\right) , \tag{C.18}$$

where $\nu = \mu/\rho_0$ is the kinematic viscosity assumed to be constant. Also using equation (C.16) in the momentum equation we get

$$\frac{Du_i}{Dt} = -\frac{\varepsilon}{\Delta\tilde{\rho}}\frac{\partial p}{\partial x_i} - \varepsilon\left[\frac{\rho}{\Delta\tilde{\rho}}\right]g\delta_{i3} + b_i + \nu\frac{\partial^2 u_i}{\partial x_j^2} . \tag{C.19}$$

The second term of the right hand side of the momentum equation (C.19) appears to be of $O\left(\varepsilon^2\right)$. In the absence of forcing $(b_i = 0)$, the system is driven by density fluctuations. This term contains the fluctuating component of density, and thus the characteristic acceleration of the fluid will be of the order $O\left(\varepsilon\left[\rho/\Delta\tilde{\rho}\right]g\right)$. This forces the conclusion that the acceleration by gravity is much larger than the characteristic acceleration that offsets the second $|\rho/\Delta\tilde{\rho}| \leq \varepsilon$ term [Spiegel and Veronis, 1960].

C.3.3 Density Equation

By using the Boussinesq approximation, it is assumed that density fluctuations are only due to temperature fluctuations and not due to pressure effects. Thus in the equation of state (2.8), density is a function of temperature only. Using equation (C.4) along with the fact that fluctuations in density are small, the relationship between temperature and density is linearized. The evolution equation of density for a fluid particle by combining internal energy equation with the equation of state is,

$$\frac{D\rho}{Dt} = D_m \frac{\partial^2 \rho}{\partial x_i^2} , \tag{C.20}$$

where $D_m = k_T / (\rho_0 C_p)$ is the mass diffusivity. Upon substituting equation (C.2) in equation (C.20) the evolution equation for density is,

$$\frac{\partial \rho}{\partial t} + u_i \frac{\partial \rho}{\partial x_i} + u_i \frac{d\tilde{\rho}(z)}{dx_i} \delta_{i3} = D_m \frac{\partial^2 \rho}{\partial x_i^2} . \tag{C.21}$$

C.3.4 Kinetic Energy

The kinetic energy is obtained by the dot product of $\vec{u}$ with the momentum equation (2.15). Since the Boussinesq approximation of continuity equation is $\partial u_i / \partial x_i = 0$, the $\nu(\partial^2 u_i / \partial x_j^2)$ term in the momentum equation is written in terms of S_{ij} (using equation (A.13)) to give the final kinetic energy equation as,

$$\frac{\partial \mathcal{E}_k}{\partial t} + \frac{\partial}{\partial x_j}(u_j \mathcal{E}_k) = -\frac{u_i}{\rho_0}\frac{\partial p}{\partial x_i} - \frac{\rho}{\rho_0}u_i g \delta_{i3} + u_i b_i + 2\nu u_i \frac{\partial S_{ij}}{\partial x_j} . \tag{C.22}$$

where $\mathcal{E}_k = \frac{1}{2}u^2$ is the kinetic energy per unit mass. Using the identity described in equation (A.14), the last term, $2\nu u_i(\partial S_{ij}/\partial x_j)$ is rewritten as

$$2\nu u_i \frac{\partial S_{ij}}{\partial x_j} = 2\nu \frac{\partial}{\partial x_j}(u_i S_{ij}) - \epsilon_k . \tag{C.23}$$

Where

$$\epsilon_k \equiv 2\nu S_{ij}S_{ij} \qquad (C.24)$$

is known as the dissipation of kinetic energy.

APPENDIX D

HORIZONTAL AND VERTICAL CONTRIBUTIONS TO KINETIC ENERGY

Equation for kinetic energy is derived by the dot product of velocity with the momentum equation. The momentum equation (2.15) restated is,

$$\frac{Du_i}{Dt} = -\frac{1}{\rho_0}\frac{\partial p}{\partial x_i} - \frac{\rho}{\rho_0}g\delta_{i3} + b_i + 2\nu\frac{\partial S_{ij}}{\partial x_j} \ . \tag{D.1}$$

Kinetic energy ($\mathcal{E}_k$) is decomposed into horizontal and vertical contributions respectively as,

$$\begin{aligned}
\mathcal{E}_h &\equiv \ \tfrac{1}{2}\left(u_1 u_1 + u_2 u_2\right) \ , \\
\mathcal{E}_v &\equiv \ \tfrac{1}{2}\left(u_3 u_3\right) \ .
\end{aligned} \tag{D.2}$$

Horizontal components (or contributions) are denoted by subscript $_h$ and for a vector $(\vec{\cdot})_h$ implies $h = 1, 2$. With this notation, horizontal component of velocity, $u_h = [u_1, u_2]$ and $\mathcal{E}_h = (1/2)u_h u_h$. Vertical components (or contributions) are denoted by subscript $_v$ and for a vector $(\vec{\cdot})_v = (\vec{\cdot})_3$.

The evolution equation for $\mathcal{E}_h$ is obtained by the dot product of horizontal component of velocity with the horizontal momentum equation. Similarly equation for $\mathcal{E}_v$ is obtained by the dot product of vertical component of velocity with the vertical momentum equation. For an incompressible flow, equations for $\mathcal{E}_h$ and $\mathcal{E}_v$ are

$$\frac{D\mathcal{E}_h}{Dt} = -\frac{u_h}{\rho_0}\frac{\partial p}{\partial x_h} + b_h + 2\nu u_h\frac{\partial S_{hj}}{\partial x_j} \ , \tag{D.3}$$

$$\frac{D\mathcal{E}_v}{Dt} = -\frac{u_3}{\rho_0}\frac{\partial p}{\partial x_3} + b_v + 2\nu u_3\frac{\partial S_{3j}}{\partial x_j} - \frac{\rho}{\rho_0}gu_3 \ . \tag{D.4}$$

τ_{ij} is a symmetric stress tensor, with Navier-Stokes assumptions it is expressed in equation (A.11). For an incompressible fluid, $\tau_{ij} = 2\mu S_{ij}$. The tensor, $\partial u_i / \partial x_j$ can be decomposed into symmetric and anti-symmetric part as,

$$\frac{\partial u_i}{\partial x_j} = \frac{1}{2}\left(\frac{\partial u_i}{\partial x_j} + \frac{\partial u_j}{\partial x_i}\right) + \frac{1}{2}\left(\frac{\partial u_i}{\partial x_j} - \frac{\partial u_j}{\partial x_i}\right) \ , \tag{D.5}$$

$$= \frac{1}{2}\left(\frac{\partial u_i}{\partial x_j}\right)_{sym} + \frac{1}{2}\left(\frac{\partial u_i}{\partial x_j}\right)_{asym} \ , \tag{D.6}$$

$$= S_{ij} + r_{ij} \ . \tag{D.7}$$

r_{ij} is the angular-deformation rate tensor. It is an anti-symmetric tensor. The product of a symmetric tensor (such as S_{ij}) with an anti-symmetric tensor (such as r_{ij}) is a null tensor. Thus,

$$S_{ij}\frac{\partial u_i}{\partial x_j} = S_{ij}S_{ij} + \cancelto{0}{S_{ij}r_{ij}} \ . \tag{D.8}$$

However, S_{hj} and S_{3j} independently are not symmetric. Therefore,

$$2\nu S_{hj}\frac{\partial u_h}{\partial x_j} = 2\nu S_{hj}S_{hj} + 2\nu S_{hj}r_{hj} \ , \tag{D.9}$$

$$2\nu S_{3j}\frac{\partial u_3}{\partial x_j} = 2\nu S_{3j}S_{3j} + 2\nu S_{3j}r_{3j} \ . \tag{D.10}$$

Noting the above equations, the viscous work term appearing in the kinetic energy equations are split as

$$2\nu u_h\frac{\partial S_{hj}}{\partial x_j} = 2\nu\frac{\partial}{\partial x_j}\left(u_h S_{hj}\right) - \left(2\nu S_{hj}S_{hj} + 2\nu S_{hj}r_{hj}\right) \ , \tag{D.11}$$

$$2\nu u_3\frac{\partial S_{3j}}{\partial x_j} = 2\nu\frac{\partial}{\partial x_j}\left(u_3 S_{3j}\right) - \left(2\nu S_{3j}S_{3j} + 2\nu S_{3j}r_{3j}\right) \ . \tag{D.12}$$

Since, $\mathcal{E}_k = \mathcal{E}_h + \mathcal{E}_v$, by adding equations (D.3) and (D.4) the total kinetic energy equation (2.20) is recovered. Terms, $2\nu S_{hj}r_{hj}$ and $2\nu S_{3j}r_{3j}$ do not appear in the total kinetic energy equation therefore,

$$S_{hj}r_{hj} = -S_{3j}r_{3j} \, . \tag{D.13}$$

Thus with equations, (D.3), (D.4), (D.11), (D.12) and (D.13) the equation for the horizontal and vertical contribution of kinetic energy is presented in equations (2.26) and (2.27)

APPENDIX E

SPECTRAL EQUATIONS

E.1 Momentum Equation

Let $(\hat{\cdot})$ denote fourier transform along the three spatial directions of $(\cdot)$. fourier transformation of the momentum equation (2.18) is,

$$\frac{\partial}{\partial t}\hat{u}_i(\vec{\kappa}, t) = \hat{A}_i(\vec{\kappa}, t) + \hat{Z}_i(\vec{\kappa}, t) + \hat{D}_i(\vec{\kappa}, t) + \hat{b}_i(\vec{\kappa}, t) - \hat{B}_i(\vec{\kappa}, t) . \tag{E.1}$$

Similarly the Fourier transform of the continuity equation (2.14) is,

$$\kappa_i \hat{u}_i = 0 . \tag{E.2}$$

κ_i is the ith component of the three dimensional wave-vector, $\vec{\kappa}$. It is possible to eliminate $\hat{Z}_i$. Taking the dot product of equation (E.1) with $\vec{\kappa}$ and using the continuity relation (E.2) gives,

$$0 = \kappa_i \left(\hat{A}_i - \hat{B}_i \right) + \kappa_i \hat{Z}_i . \tag{E.3}$$

Substituting for $\hat{Z}_i$ from equation (2.19) yields,

$$\left(\widehat{\frac{p_t}{\rho_0} + \frac{u_j u_j}{2}} \right) = \frac{\kappa_i}{\kappa^2} \left(\hat{A}_i - \hat{B}_i \right) . \tag{E.4}$$

$\kappa \equiv |\vec{\kappa}|$ is the magnitude of the wave-number. Substituting (E.4) into (E.1) gives,

$$\frac{\partial \hat{u}_i}{\partial t} = \hat{A}_i - \hat{B}_i + \frac{\kappa_i \kappa_j}{\kappa^2} \left(\hat{A}_j - \hat{B}_j \right) + \hat{D}_i + \hat{b}_i . \tag{E.5}$$

Thus the Fourier space momentum equation for forced density stratified flows is,

$$\frac{\partial \hat{u}_i}{\partial t} = \Lambda_{ij} \left(\hat{A}_j - \hat{B}_j \right) - \nu \kappa^2 \hat{u}_i + \hat{b}_i \ . \tag{E.6}$$

Where $\hat{\vec{A}} \equiv \widehat{(\vec{u} \times \vec{\omega})}$ and $\Lambda_{ij} \equiv [\delta_{ij} - (\kappa_i \kappa_j)/\kappa^2]$. The momentum equation including hyper-viscosity (defined by Lindborg [2006]) is,

$$\frac{\partial \hat{u}_i}{\partial t} = \Lambda_{ij} \left(\hat{A}_j - \hat{B}_j \right) - \nu \kappa^2 \hat{u}_i + \left(\nu_h \left(\kappa_1^2 + \kappa_2^2 \right)^4 + \nu_v \kappa_3^8 \right) \hat{u}_i + \hat{b}_i \ . \tag{E.7}$$

For isotropic-homogeneous flows, $\hat{B}_i = 0$ thus,

$$\frac{\partial \hat{u}_i}{\partial t} = \Lambda_{ij} \hat{A}_j - \nu \kappa^2 \hat{u}_i + \hat{b}_i \ . \tag{E.8}$$

E.2 Kinetic Energy Equation

The Fourier space kinetic energy ($\hat{E}_k \equiv \hat{u}_i \hat{u}_i^* / 2$) equation is obtained by the dot product of equation (2.30) with the complex-conjugate of velocity vector ($\hat{u}_i^*$). Equation for kinetic energy is,

$$\frac{\partial \hat{E}_k(\vec{\kappa}, t)}{\partial t} = \Lambda_{ij} \left(\hat{A}_j - \hat{B}_j \right) \hat{u}_i^* - \nu \kappa^2 \hat{E}_k(\vec{\kappa}, t) + \hat{b}_i \hat{u}_i^* \ . \tag{E.9}$$

From continuity relation, $\kappa_i \hat{u}_i = \kappa_i \hat{u}_i^* = 0$, the dot product $\Lambda_{ij} \hat{u}_i^*$ simplifies to

$$\Lambda_{ij} \hat{u}_i^* = \left[\delta_{ij} - \frac{\kappa_i \kappa_j}{\kappa^2} \right] \hat{u}_i^* \ , \tag{E.10}$$

$$= \delta_{ij} \hat{u}_i^* - \frac{\kappa_i \hat{u}_i^* \kappa_j}{\kappa^2}^{\nearrow 0} \ , \tag{E.11}$$

$$= \hat{u}_i^* \ . \tag{E.12}$$

The equation for Fourier space kinetic energy is conveniently written as,

$$\frac{\partial \hat{E}_k(\vec{\kappa}, t)}{\partial t} = \hat{T}_k(\vec{\kappa}, t) + \hat{T}_b(\vec{\kappa}, t) - \hat{T}_B(\vec{\kappa}, t) - \hat{T}_{\epsilon_k}(\vec{\kappa}, t) \,. \tag{E.13}$$

Where

$$\begin{aligned}
\hat{T}_k(\vec{\kappa}, t) &\equiv \frac{1}{2}\left(\hat{A}_j \hat{u}_i^* + \hat{A}_j^* \hat{u}_i\right) \,, \\
\hat{T}_b(\vec{\kappa}, t) &\equiv \frac{1}{2}\left(\hat{b}_i \hat{u}_i^* + \hat{b}_i^* \hat{u}_i\right) \,, \\
\hat{T}_B(\vec{\kappa}, t) &\equiv \frac{g}{2\rho_0}\left(\hat{\rho} \hat{u}_3^* + \hat{\rho}^* \hat{u}_3\right) \,, \\
\hat{T}_{\epsilon_k}(\vec{\kappa}, t) &\equiv -\nu \kappa^2 \hat{E}_k\left(\vec{\kappa}, t\right) \,, \\
\hat{T}_{hk}(\vec{\kappa}, t) &\equiv \left(\nu_h \left(\kappa_1^2 + \kappa_2^2\right)^4 + \nu_v \kappa_3^8\right) \hat{E}_k(\vec{\kappa}, t) \,, \\
\hat{T}_{\epsilon_k h}(\vec{\kappa}, t) &\equiv \hat{T}_{\epsilon_k} + \hat{T}_{hk} \,.
\end{aligned} \tag{E.14}$$

With the inclusion of hyper-viscosity, the kinetic energy equation is

$$\frac{\partial \hat{E}_k(\vec{\kappa}, t)}{\partial t} = \hat{T}_k(\vec{\kappa}, t) - \hat{T}_B(\vec{\kappa}, t) + \hat{T}_b(\vec{\kappa}, t) + \hat{T}_{\epsilon_k h}(\vec{\kappa}, t) \,. \tag{E.15}$$

For isotropic homogeneous flows $\hat{T}_B = 0$, the kinetic energy equation is,

$$\frac{\partial \hat{E}_k(\vec{\kappa}, t)}{\partial t} = \hat{T}_k(\vec{\kappa}, t) + \hat{T}_b(\vec{\kappa}, t) + \hat{T}_{\epsilon_k}(\vec{\kappa}, t) \,. \tag{E.16}$$

E.3 Density and Potential Energy Equation

Equation (2.13) for density multiplied with scaling $\mathcal{C} = -g/\left(2\rho_0(d\tilde{\rho}/dz)\right)$ is,

$$\mathcal{C}\frac{\partial \rho}{\partial t} + \mathcal{C} u_i \frac{\partial \rho}{\partial x_i} - \frac{g}{\rho_0} u_3 = \mathcal{C} D_m \nabla^2 \rho \,. \tag{E.17}$$

Fourier transforming this equation gives,

$$\mathcal{C}\frac{\partial\hat{\rho}}{\partial t} + \left(\widehat{\mathcal{C}u_i\frac{\partial\rho}{\partial x_i}}\right) - \frac{g}{\rho_0}\hat{u}_3 = -\mathcal{C}D_m\kappa^2\hat{\rho}\,. \qquad (E.18)$$

Multiplying above equation with the complex conjugate of $\hat{\rho}$ gives,

$$\mathcal{C}\frac{\partial}{\partial t}\left(\hat{\rho}^*\hat{\rho}\right) = -\hat{\rho}^*\left(\widehat{\mathcal{C}u_i\frac{\partial\rho}{\partial x_i}}\right) + \frac{g}{\rho_0}\hat{\rho}^*\hat{u}_3 - D_m\kappa^2\mathcal{C}\hat{\rho}^*\hat{\rho}\,.$$

Calling

$$\hat{E}_p(\vec{\kappa},t) \equiv \mathcal{C}\hat{\rho}^*\hat{\rho}\,, \qquad (E.19)$$

$$\hat{T}_p(\vec{\kappa},t) \equiv \frac{1}{2}\left(\hat{\rho}^*\left(\widehat{\mathcal{C}u_i\frac{\partial\rho}{\partial x_i}}\right) + \hat{\rho}\left(\widehat{\mathcal{C}u_i\frac{\partial\rho}{\partial x_i}}\right)^*\right)\,,$$

$$\hat{T}_{\epsilon_p}(\vec{\kappa},t) \equiv -D_m\kappa^2\hat{E}_p\,,$$

the spectral form of potential energy is,

$$\frac{\partial\hat{E}_p(\vec{\kappa},t)}{\partial t} = -\hat{T}_p(\vec{\kappa},t) + \hat{T}_B(\vec{\kappa},t) + \hat{T}_{\epsilon_p}(\vec{\kappa},t)\,. \qquad (E.20)$$

APPENDIX F

THE PHASE FOR VECTOR

F.1 Derivation for Phase of Velocity Component: θ_u

Velocity vector in Fourier space is, $\hat{u}_i(\kappa_1, \kappa_2, \kappa_3, t)$ and the divergence condition is,

$$\kappa_i \hat{u}_i = 0. \tag{F.1}$$

For horizontally homogeneous isotropic forcing, only the horizontal components of velocity in the horizontal Fourier plane $\kappa_3 = 0$ are forced. Thus for this plane the divergence condition is,

$$\kappa_1 \hat{u}_1 + \kappa_2 \hat{u}_2 = 0,$$

where $\hat{u}_1 = a_1 + ib_1$ and $\hat{u}_2 = a_2 + ib_2$ are the complex horizontal components of the velocity field. Let $|\cdots|_c$ denote the magnitude of a complex number. Then the horizontal components of the velocity vector can be written as,

$$\hat{u}_1 = |\hat{u}_1|_c e^{i\theta_1}, \tag{F.2}$$

$$\hat{u}_2 = |\hat{u}_2|_c e^{i\theta_2}, \tag{F.3}$$

where

$$\theta_i = \tan^{-1}\left(\frac{b_i}{a_i}\right) \quad \text{for } i = 1, 2. \tag{F.4}$$

is the phase for each of the horizontal component of velocity. Applying divergence condition yields,

$$a_2 = a_2 \frac{\kappa_2}{\kappa_1} \ , \tag{F.5}$$

$$b_2 = b_2 \frac{\kappa_2}{\kappa_1} \ . \tag{F.6}$$

From this it can be seen that $\theta_1 = \theta_2 = \theta_u$.

BIBLIOGRAPHY

K. Alvelius. Random forcing of three-dimensional homogeneous turbulence. *Phys. Fluids*, 11: 1880–1889, 1999.

R. Aris. *Vector Tensors and the Basic Equations of Fluid Mechanics*. Prentice Hall, New Jersey, 1962.

G. K. Batchelor. *Homogeneous Turbulence*. Cambridge University Press, London, 1956.

R. Byron Bird, Warren E. Stewart, and Edwin N. Lightfoot. *Transport Phenomena*. Wiley, New York, second edition, 2002.

J. Boussinesq. *Théorie analytique de la chaleur*, volume 2, p. 172. Gauthier-Villars, Paris, 1903.

J. P. Boyd. *Chebyshev and Fourier Spectral Methods*. Dover, 2001.

D. Carati, S. Ghosal, and P. Moin. On the representation of backscatter in dynamic localization models. *Phys. Fluids*, 7(3):606–616, 1995.

J. R. Chasnov. Simulation of the Kolmogorov inertial subrange using an improved subgrid model. *Phys. Fluids A*, 3:188–200, 1991.

X. Chen, S. Shan. High-resolution turbulent simulations using the Connection Machine-2. *Comput. Phys.*, 6:643–646, 1992.

G. Comte-Bellot and S. Corrsin. Simple Eulerian time correlation of full and narrow-band velocity signals in grid-generated 'isotropic' turbulence. *J. Fluid Mech.*, 48:273–337, 1971.

S. M. de Bruyn Kops and J. J. Riley. Direct numerical simulation of laboratory experiments in isotropic turbulence. *Phys. Fluids*, 10(9):2125–2127, 1998.

V. Eswaran and S. B. Pope. Direct numerical simulations of the turbulent mixing of a passive scalar. *Phys. Fluids*, 31:506–520, 1988.

S. Ghosal, T. S. Lund, P. Moin, and K. Akselvoll. A dynamic localization model for large-eddy simulation of turbulent flows. *J. Fluid Mech.*, 286:229–255, 1995.

S. Grossmann and D. Lohse. Scaling in hard turbulent Rayleigh-Benard Flow. *Phys. Rev. A*, 46: 903–917, 1992.

D. Holliday and M. McIntyre. On potential energy density in an incompressible, stratified fluid. *J. Fluid Mech.*, 107:221–225, 1981.

W. Hwang and J. K. Eaton. Creating homogeneous and isotropic turbulence without a mean flow. *Exp. Fluids*, 36:444–454, 2004.

R. M. Kerr. *Theoretical Investigation of a Passive Scalar such as Temperature in Isotropic Turbulence*. PhD thesis, Cornell University, 1981.

R. M. Kerr. Higher-order derivative correlations and the alignment of small-scale structures in isotropic turbulence. *J. Fluid Mech.*, 153(31):31, 1985.

A. K. Kuczaj and B. J. Geurts. Mixing in manipulated turbulence. *J. Turbulence*, 7:1–28, 2006.

P. K. Kundu and I. M. Cohen. *Fluid Mechanics*. Academic Press, 2nd edition, 2002.

E. Lindborg. The energy cascade in a strongly stratified fluid. *J. Fluid Mech.*, 550:207–242, 2006.

E. N. Lorenz. Available potential energy and the maintenance of the general circulation. *Tellus*, 7: 157–167, 1955.

T. S. Lundgren. Linearly forced isotropic turbulence. In *Annual Research Briefs 2003*, pages 461–473. Center for Turbulence Research, 2003.

L. Machiels. Predictability of small-scale motion in isotropic fluid turbulence. *Phys. Rev. Lett.*, 79: 3411–3414, 1997.

A. Misra and D. I. Pullin. A vortex-based subgrid stress model for large-eddy simulation. *Phys. Fluids*, 9:2443–2454, 1997.

M. R. Overholt and S. B. Pope. A deterministic forcing scheme for direct numerical simulations of turbulence. *Comput. Fluids*, 27:11–28, 1998.

R. L. Panton. *Incompressible Flow*. John Wiley & Sons, New York, 1984.

J. B. Perot. Determination of the decay exponent of mechanically stirred isotropic turbulence. *Fluids Dynamics Research*, 2010(submitted).

S. B. Pope. *Turbulent Flows*. Cambridge University Press, Cambridge, 2000.

William Prager. *Introduction to Mechanics of Continua*. Boston, Ginn and Company, 1961.

J. J. Riley and S. M. de Bruyn Kops. Dynamics of turbulence strongly influenced by buoyancy. *Phys. Fluids*, 15(7):2047–2059, 2003.

C. Rosales and C. Meneveau. Linear forcing in numerical simulations of isotropic turbulence: Physical space implementations and convergence properties. *Phys. Fluids*, 17(9), 2005.

E. D. Siggia and G. S. Patterson. Intermittency effects in a numerical-simulation of stationary 3-dimensional turbulence. *J. Fluid Mech.*, 86:567–592, 1978.

E. A. Spiegel and G. Veronis. On the Boussinesq approximation for a compressible fluid. *Astrophys J.*, 131:442–447, 1960.

N. P. Sullivan, Mahalingam S., and R. M. Kerr. Deterministic forcing of homogeneous, isotropic turbulence. *Phys. Fluids*, 6(4):1612–1614, 1994.

E. A. Variano and E. A. Cowen. A random-jet-stirred turbulence tank. *J. Fluid Mech.*, 604:1–32, 2008.

E. A. Variano, E. Bodenschatz, and E. A. Cowen. A random synthetic jet array driven turbulence tank. *Exp. Fluids*, 37:613–615, 2004.

A. Vincent and M. Meneguzzi. The spatial structure and statistical properties of homogeneous turbulence. *J. Fluid Mech.*, 225:1–20, 1991.

H. Wang and W. K. George. The integral scale in homogeneous isotropic turbulence. *J. Fluid Mech.*, 459:429–443, 2002.

L. P. Wang, S. Y. Chen, J. G. Brasseur, and J. C. Wyngaard. Examination of hypotheses in the Kolmogorov refined turbulence theory through high-resolution simulations. Part 1. Velocity field. *J. Fluid Mech.*, 309:113–156, 1996.

K. B. Winters, P. N. Lombard, J. J. Riley, and E. A. D'Asaro. Available potential energy and mixing in density-stratified fluids. *J. Fluid Mech.*, 289:115–128, 1995.

C. S. Yih. *Fluid Dynamics*. McGraw-Hill, 1974.